Trinity River Restoration Program

DRAFT Technical Report: TR-TRRP-2019-2

WY2015 Trinity River Gravel Augmentation Implementation Monitoring Report

Prepared by:

David Gaeuman[1] and Robert Stewart[2]
Trinity River Restoration Program
Weaverville, California

[1]Yurok Tribe Fisheries Department, Trinity River Division, Weaverville, CA
[2]Civil & Environmental Consultants, Inc., Bridgeport, WV

April 2019

Contents

Abstract

The loss of a natural gravel supply to the Trinity River downstream from Lewiston Dam has been implicated as contributing to decreases in salmonid populations following dam construction. A supply of mobile gravel is necessary to sustain the fluvial processes that create diverse physical habitats that support all salmon life stages, as well as a wide range of other riverine species. Artificial gravel augmentation is among the strategies employed by the Trinity River Restoration Program (TRRP) to recover salmonid populations in the river. However, the rate and manner in which augmented gravel will alter downstream habitats, as well as the potential risks associated with gravel augmentation, are imperfectly known. This report presents the results of site-specific monitoring performed at two sites where gravel augmentations were implemented in water year (WY) 2015, as well as an investigation of photographic methods for assessing system-wide changes in substrate conditions over time.

In 2015, repeat topographic surveys were conducted to assess geomorphic responses to high-flow gravel injections at the Diversion Pool, where 1000 yd^3 of gravel was injected during the spring high-flow release, and at Lowden Ranch, where 680 yd^3 of gravel was injected. Earlier studies have indicated that most of the gravel injected at the Diversion Pool prior to 2015 was deposited on the inside of a bend a short distance downstream from the injection point. The current analysis, however, provides the first clear evidence that gravel stored in that region has remobilized and propagated into the next reach downstream. At Lowden Ranch, the 2015 data show that virtually none of the gravel injected at that site during the 2015 flow release or delivered from upstream was transported more than about 1000 ft downstream from the injection point. Half of the total gravel load at the injection point deposited in the form of a lateral bar along the left bank immediately downstream, and half was deposited in the form of a series of gravel dunes that formed early in the flow release. Geomorphic changes during the release resulted in a modest increase in topographic variability and planform complexity in the subreach immediately downstream from the injection point. Another subreach upstream from the injection point aggraded substantially. Most of the changes observed in these reaches occurred in the first hours of the hydrograph peak. Notable geomorphic changes were absent in two other portions of the Lowden Ranch site, even though a large gravel flux was transmitted through one of them. No adverse consequences of the 2015 gravel injections at either site were identified. We recommend that both the Diversion Pool and the Lowden Ranch injection locations continue to be regarded as the default locations for implementing future high-flow gravel injections.

Structure-for-motion photography was determined to be an effective means for developing orthorectified images of the bed surface over areas large enough to support grain size analysis. Comparisons between field pebble counts and pebble counts on the ortho-images indicate that the image-based measurements tend to be biased low, but typically differ from the field measurements by less than 10%. A computer script designed to automatically extract particle size information from photographs was found to produce unacceptable results. Its use is not recommended.

Introduction

The Trinity River downstream from Lewiston, California, has been regulated since Trinity Dam was closed in the fall of 1960, followed by the initiation of flow diversions from Lewiston Dam to the Sacramento River basin in 1963. Dams alter downstream physical conditions by altering streamflow and by cutting off the supply of bed-material sediments from upstream, potentially leading to channel incision, coarsening of the streambed, and decreased bed mobility (Williams and Wolman 1984; Church 1995). Such changes have been implicated as contributing to post-dam decreases in salmonid populations in the Trinity River (USFWS and HVT 1999), and led to the establishment of the Trinity River Restoration Program (TRRP) in 2002. The TRRP restoration strategy is based on the hypothesis that recovery of the fishery can be achieved by encouraging fluvial processes such as scour, bar deposition, and planform change that create and maintain complex physical habitat in the river. Four types of management action are available to the TRRP for promoting these processes: mechanical rehabilitation, flow management, fine sediment source control, and coarse sediment augmentation (USDOI 2000). This report is focused on monitoring activities that are specifically intended to evaluate the results of coarse sediment augmentations.

Coarse sediment augmentations in the Trinity River are implemented for geomorphic purposes (USFWS and HVT 1999; USDOI 2000). That is, the intent is to supply gravel at a rate and with a particle size distribution that will support the geomorphic processes that maintain substrate quality and physical habitat integrity. Trinity River augmentations are currently designed to supply gravel and small cobble to the reaches downstream from Lewiston Dam at a rate equal to or slightly greater than the rate at which those sediment fractions can be transported downstream (Gaeuman 2014b). For brevity, these sediment size classes are henceforward referred to as “gravel.” It is hypothesized that gravel augmentations will decrease bed surface particle sizes and increase bed mobility, thereby stimulating increased rates of geomorphic activity (Dietrich et al. 1989). Processes such as bed scour and fill, bank erosion, and channel migration are thought to benefit the riverine ecosystem by improving substrate conditions, creating diverse aquatic habitats, and rejuvenating the riparian zone (Petts and Maddock 1996; Kondolf and Wilcock 1996; Stanford 1996; Richter et al. 1997; Milhous 1998). Although such changes are initially expected only near the location where the material is added to the river, the effects of sustained gravel augmentations are expected to propagate farther downstream over time and eventually improve habitat conditions throughout the upper reaches of the river. In addition to producing habitat benefits, increasing the gravel supply can also have unintended consequences. For example, local increases in gravel deposition can increase flood risks, stimulate unwanted bank erosion, interfere with navigation, and even decrease habitat complexity by filling pools. Regardless of whether these various outcomes are considered to be positive or negative, it is incumbent on resource managers to be aware of them and attempt to anticipate them. The current state of the science, however, is inadequate to confidently predict precisely where and when these various potential outcomes will be realized (Lisle et al. 1997; Sklar et al. 2009; Humphries et al. 2012). Direct monitoring of changes in stream topography, substrate condition, and habitat quality is therefore necessary for TRRP to assess the consequences of past gravel augmentations and fulfill its mandate to continuously improve its restoration practices through an adaptive management process.

As gravel augmentation in the Trinity River are intended to improve aquatic habitat by increasing topographic complexity, the outcome of gravel augmentations is primarily monitored with topographic surveys that document morphologic change and quantify channel complexity. This report presents the results of topographic monitoring performed in reaches downstream from where gravel augmentations were implemented in water year (WY) 2015.

Another way gravel augmentations are expected to achieve the basic objective of promoting fluvial processes is by decreasing sediment particle sizes on the river bed, thereby increasing bed-material mobility. Thus, gravel augmentation monitoring included efforts to assess long-term changes in bed surface grain sizes upstream from Indian Creek. One approach to substrate monitoring that TRRP has explored consists of documenting bed surface particle sizes by photographing the surfaces of gravel bars. Work of this type was initiated in WY 2014, when digital photographs were obtained near the baseflow waterline at the upstream ends of 55 gravel bars in the river reaches between Lewiston Dam and Indian Creek (GMA 2015). The intent of this data collection effort was to create a baseline record of substrate conditions that can be compared with future conditions to quantify changes over time. It has been hypothesized that continued gravel augmentation will eventually cause bar-surface grain sizes to decrease, and that this effect will be observed at greater distances downstream from the gravel augmentation locations over time (TRRP and ESSA 2009). These types of changes will be evident in comparisons between the 2014 photos and newer photos obtained in later years, provided the changes are sufficiently large.

Substrate monitoring in 2014 also included the collection of field pebble counts on a subset of the bars photographed. These pebble counts were intended to provide a basis for assessing the degree to which grain-size distributions obtained from measurements on photographs deviate from grain-size distributions measured in the field. Initial results revealed unexpectedly large discrepancies between the field and photo-based measurements. Due to uncertainty in the validity of the results, as well as the continued drought that made substrate changes unlikely, this form of substrate monitoring was suspended in 2015. By 2016, however, TRRP had acquired advanced image processing software that opens new possibilities for obtaining and processing photographic substrate samples.

Flow and Gravel Management

The TRRP manages gravel supplies in a segment of the Trinity River that extends from Lewiston Dam to Indian Creek, located 16.4 river miles downstream (Figure 1). According to scientific studies and administrative documents that established the Program (USFWS and HVT 1999; USDOI 2000), the cumulative sediment deliveries from Indian Creek and upstream tributaries are sufficiently large that gravel augmentation is unnecessary downstream from that point.

Flow Management

The behavior of sediment in a stream is critically dependent on water flow, so any discussion of gravel management must include consideration of flow management. The record of decision issued by the US Department of the Interior that authorized establishment of the

TRRP (USDOI 2000) defines five annual hydrographs, each of which corresponds to a water year type – critically dry, dry, normal, wet, and extremely wet – defined according to the total water yield from the Trinity River catchment upstream from the dams (Table 1). Each water year type is associated with a cumulative probability that it will be exceeded in any given water year, and each of the five hydrographs specifies a total water volume available for release from Lewiston Dam for that water year and a recommended peak magnitude for the annual spring high-flow release.

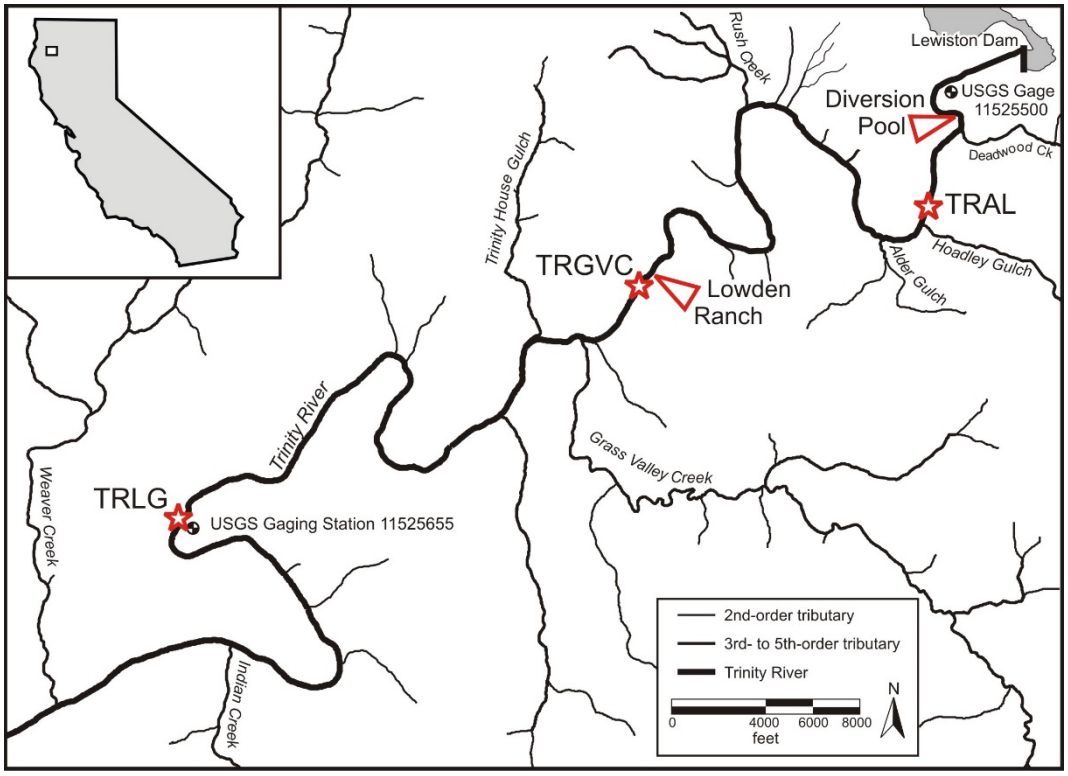

Figure 1: Map of the Trinity River between Lewiston Dam and Weaver Creek. Red triangles point to gravel injection locations referred to in the text; red stars labelled TRAL, TRGVC, and TRLG indicate stream gaging and sediment monitoring locations discussed in the methods section.

Table 1: Water year and release hydrograph types defined for Trinity River management. Catchment yield thresholds and release volumes are given in thousand acre-ft (Kaf).

WY Type	Critically Dry	Dry	Normal	Wet	Extremely Wet
Catchment Yield (Kaf)	--	650	1025	1350	2000
Probability	0.12	0.28	0.20	0.28	0.12
Release Volume (Kaf)	369	453	647	701	815
Nominal Release Peak (cfs)	1500	4500	6000	8500	11000

Water year 2011 was classified as a wet year, but TRRP chose to maximize geomorphic change by releasing the largest peak flow authorized by the record of decision of 11000 ft^3/s

(due to operational issues, the maximum daily mean flow peaked at 11,600 ft^3/s). Flow releases in the three years following 2011, however, were relatively small due to a prolonged drought that affected most of California. The largest release in that time frame took place in 2012, when a peak flow magnitude of about 6000 ft^3/s was released for about three days (Figure 2). Releases in 2013 and 2014 were even smaller. The drought continued into WY 2015, which was classified as a dry year in terms of catchment yield. But in 2015, TRRP again opted to stimulate geomorphic change by releasing a higher peak flow than is typically prescribed for that water year type. The dry-year release volume available in 2015 was compressed into a flow release hydrograph with a relatively high, but brief peak that remained near 8600 ft^3/s for about 2½ days (Figure 2).

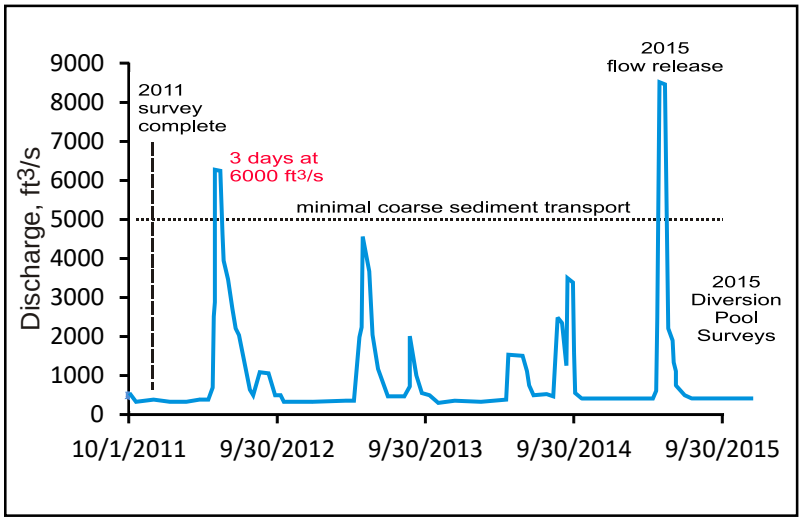

Figure 2: Trinity River flow releases from Lewiston Dam from the fall of 2011 through the summer of 2015. Differences between the magnitudes of dam releases and flows gaged at Lowden Ranch (TRGVC, Figure 1) are negligible.

Gravel Augmentations

Since its inception, TRRP has used two basic methods to implement gravel augmentations: direct injection of gravel into the main flow during high-flow releases from Lewiston Dam and construction of in-channel bars in association with channel rehabilitation projects. As of the end of WY 2015, the majority (69%) of all TRRP gravel additions implemented upstream from Indian Creek had been associated with bar construction. In those cases, the quantity of gravel added to a site depends on the specific objectives of the restoration design being implemented. By the end of 2010, however, most of the sites slated for mechanical restoration upstream from Indian Creek had been completed, so high-flow injections have taken a progressively larger role in ensuring that the upper river receives an adequate supply of gravel. In 2010 and 2011, a total of 8430 yd^3 of mobile gravel was added to the river via high-flow injections at two locations – the Diversion Pool and Lowden Ranch (Figure 1). These two sites have served as the Program's default gravel injection locations since 2010 for logistical and political reasons outlined by Gaeuman (2014b).

Gravel injections were almost entirely curtailed in the three drought years spanning 2012-2014. Gravel augmentations of any kind during that time period consisted only of a single high-flow injection of 200 yd^3 at the Diversion Pool in 2013 and construction of an in-channel bar at another location in 2014. Although drought continued into 2015, the Program chose to release a larger flow than is typically recommended for dry water years, in part, to support gravel injections that would begin to make up for the lack of augmentations in the preceding three years. Consequently, a total of 1680 yd^3 of mobile gravel was introduced into the river in 2015 via high-flow injections at the Diversion Pool and Lowden Ranch (Figure 1). Gravel injections at both of these locations were implemented over a two-day period spanning the rising limb and first day of the release peak (Figure 3).

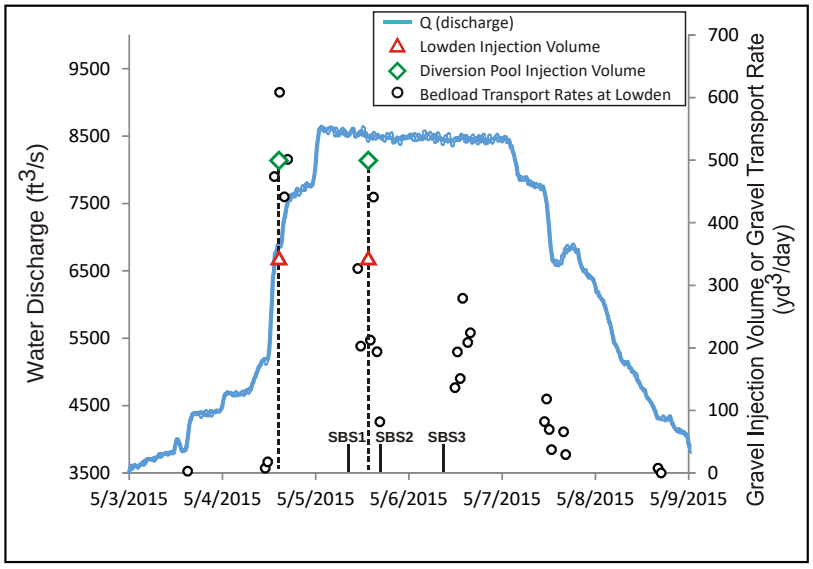

Figure 3: 2015 spring flow release hydrograph with gravel injection times and volumes and times of sonar bathymetric surveys (SBS) 1-3 indicated. Date hash marks correspond to 0:00 hours.

The Diversion Pool site, located 0.9 miles downstream from Lewiston Dam (River Mile 111.2 upstream from the Klamath River confluence), has been the most frequently used gravel augmentation site since TRRP started implementing high-flow gravel injections in 2008 (Gaeuman 2014b). As of the beginning of 2015, 55% (7465 of 13460 yd^3) of all gravel that TRRP has injected into the river during high-flow releases has been injected at the Diversion Pool.

The Diversion Pool injection point is immediately downstream from a concrete weir that spans nearly the entire valley floor and constricts flow into a narrow rapid characterized by large standing waves and strong turbulence capable of immediately entraining the injected material. A level surface above flood stage on river right is suitable for stockpiling coarse sediment and operating heavy equipment that can inject gravel directly into the main flow during flood events (Figure 4). The 2015 gravel injection at the Diversion Pool was performed by pushing about 500 yd^3 of gravel into the flow with a front-end loader during

the middle of the day on May 4 and again on May 5 (Figure 3). In all, 1000 yd^3 of gravel were injected over those two days, bringing the total volume injected at the Diversion Pool since Program inception to 8465 yd^3.

Figure 4: 2015 aerial photograph of the Diversion Pool reach of the Trinity River. The red asterisk indicates the gravel injection point and the white arrow indicates flow direction.

The Lowden Ranch gravel injection site, located about 7 miles downstream from Lewiston Dam (River Mile 104.9 upstream from the Klamath River confluence), was first used during the 2011 spring flow release, following the completion of the Lowden Ranch channel rehabilitation project in the fall of 2010. That project featured terrace lowering and minor channel widening that was explicitly intended to encourage bar deposition in response to gravel injections (Gaeuman 2014a). The 2011 injection consisted of a total gravel volume of 2050 yd^3 that was pushed into the flow from a left-bank terrace near the upstream end of the project site (Figure 5). No further gravel injections were performed at Lowden Ranch until 2015, when 680 yd^3 of gravel were injected. Half of that total was injected on May 4 and the remaining half was injected on May 5 (Figure 3). The particle size distribution of the injected gravel was similar to that of the bed surface in the reach, particularly for size fractions larger than the median. Pebble counts performed prior to the release indicated that the median and 90th percentile particle sizes of the injection material were about 64 and 121 mm, respectively, whereas the same percentiles for the bed surface were found to be 55 and 118 mm. The bed surface material, however, had a finer tail than the injection gravel (Figure 6).

Figure 5: 2015 aerial photograph of the Lowden Ranch reach of the Trinity River. The section of channel surveyed with multibeam sonar in 2015 is outlined in black. The red asterisk indicates the gravel injection point, the red line indicates the sediment transport sampling transect, and the white arrow indicates flow direction.

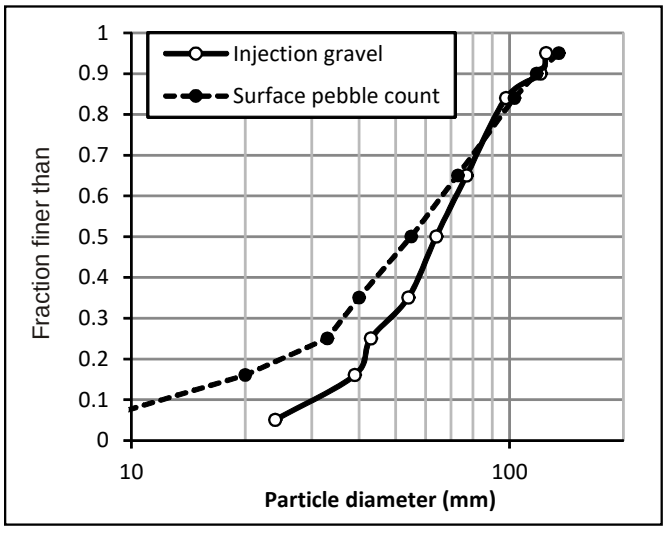

Figure 6: Particle size distribution of the gravel injected in 2015 compared with the bed surface particle size in the Lowden Ranch Reach.

Monitoring Methods

Topographic Surveys

The ultimate objective of gravel augmentation is to improve aquatic habitat by increasing topographic complexity, so the outcome of gravel augmentations is primarily monitored with topographic surveys that document morphologic change and quantify channel complexity. Rates of change can be quantified in terms of volumes of coarse bed material eroded or deposited in various locations, as determined by topographic differencing, as well as by gravel flux estimates computed from a morphology-based sediment budget (Ashmore and Church 1998). The bed of the Trinity River is composed of clast-supported gravel and cobbles (Viparelli et al. 2011), so changes in the bed material volumes determined by topographic differencing is considered to be insensitive to the presence of sand because the fine bed material fractions occupy the pore spaces between the larger grains (Gaeuman 2014a).

Change detection from topographic surveys requires a minimum of two topographic datasets collected at different times. The initial conditions dataset used for the analyses presented herein is taken from a high-resolution terrain model that covers most of the 40 miles of the Trinity River between Lewiston Dam and the North Fork Trinity River. This terrain model, which is referred to herein as the 2011 terrain model, is based on aerial LiDAR (Watershed Sciences, Inc. 2012) and continuous bathymetric sonar obtained in the summer of 2011 through the early winter of 2012 (GMA 2012). It therefore represents conditions following the large spring flow release of 2011.

Sonar for the 2011 terrain model was obtained in open water areas with depths greater than 1.5 ft using a Ross Laboratories 875-8 portable hydrographic sonar sweep system mounted on a jet boat or cataraft. The sweep system accommodates an array of seven sonar transducers spaced 3.28 ft apart. Positioning information is provided by integrated real time kinematic (RTK) GPS with multiple antennae and a Honeywell HMR 3000 attitude sensor. The single-ping precision of the sonar elevations is estimated to be less than 0.3 ft and the sonar point density exceeded two points per yd^2 (Gaeuman 2014a). The estimated precision of the LiDAR elevations incorporated in the 2011 terrain is also less than 0.3 ft and point densities are typically on the order of tens of points per yd^2. In some areas, however, neither of these technologies is effective. The sweep sonar system is unable to collect valid data in submerged areas that are less than 1.5 ft deep or in whitewater areas where bubbles interfere with sonar transmission, and the LiDAR is only useful for mapping sub-aerial surfaces. Thus, it was necessary to fill in some areas with traditional ground surveys using RTK GPS or a laser total station. But even these traditional surveys are impractical in some locations where dense vegetation limits GPS reception or sight distance or where the water is too swift for sonar and too deep for wading. The 2011 terrain model therefore includes some areas with poor data quality or even data voids.

Virtually the entire Lowden Ranch reach is accessible to the sweep sonar system, so the quality of the 2011 terrain model in that area is high. That is not the case in the Diversion Pool reach, much of which consists of a steep rapid containing large boulders and abundant whitewater upstream from the New Lewiston Bridge (Figure 4). Furthermore, the reach

downstream from the New Lewiston Bridge consists of a large heavily vegetated island and several small channels that are difficult to survey. Boat access is limited by extremely shallow flow in some channels and a narrow flow width or aerated water in others, whereas excessive canopy prevents the use of GPS. Ground-based total station surveys are also logistically difficult, due to limited sight distance and difficult terrain. Consequently, useful and reliable 2011-2012 topographic data in the Diversion Pool reach is mostly limited to the pool immediately downstream from the gravel injection point (where the arrow is in Figure 4) and to the terrestrial area on the inside of the bend upstream from the bridge.

We addressed the deficiency of reliable topographic data in the Diversion Pool reach by dedicating a high level of effort to obtaining a complete terrain model for that reach in 2015. Field crews surveyed a length of channel extending about 3000 ft downstream from the Diversion Pool gravel injection point using a combination of sonar and ground surveys over a period spanning August 2015 through March 2016. About 20% of the area was mapped using the sweep sonar system and most of the remainder was acquired with a total station to produce an elevation grid with a 3-ft horizontal resolution and a root-mean-square vertical error of 0.19 ft (GMA 2016a). This data product supports change detection between 2011-2012 and 2015 in portions of the Diversion Pool reach, but perhaps more importantly it provides a baseline for assessing future topographic changes throughout the reach as the Program continues to inject gravel at the Diversion Pool.

A large amount of new topographic data was also obtained in 2015 at the Lowden Ranch site. At that site an advance multibeam sonar technology was employed to acquire a complete high-resolution bathymetric terrain model over the entire reach at four different times during the 2015 flow release. Multiple surveys during the release make it possible to track the downstream propagation of the augmented material, whereas one could only infer the behavior of the injected material if only pre- and post-release surveys were conducted. A 400-kHz Norbit iWBMSc multibeam sonar featuring 256 sonar beams with a sampling rate of 40 Hz was used for these surveys. This instrument made it possible to collect bathmetric surveys with cm-scale resolution through a reach spanning about a half mile in 1.5 to 2 hours. All four of the multibeam surveys began about 1000 ft upstream from the high-flow gravel injection point and ended at the upstream end of a pair of islands about 1800 ft downstream from the injection point (Figure 5). Three of the surveys were conducted during the hydrograph peak – sonar bathymetric survey 1 (SBS1) was acquired on the morning of May 5, SBS2 was acquired in the late afternoon of May 5, and SBS3 was acquired the following morning on May 6 (Figure 3). A fourth multibeam survey (SBS4) was acquired in the late afternoon on May 10, after flows had decreased to about 3000 ft^3/s. Bedload sampling during the 2015 flow release shows that gravel transport in the reach is negligible when discharge falls below about 3500 ft^3/s (Figure 3). Finally, a conventional ground-based survey was conducted in a small area along the left bank immediately downstream from the gravel injection point several weeks later after discharge had receded to a summer baseflow level. That area could not be surveyed via sonar during the release due to insufficient flow depths and the presence of patchy riparian vegetation.

Integration with Sediment Monitoring

TRRP monitors sediment transport rates during the annual high-flow releases from Lewiston Dam at four locations along the Trinity River. Bedload transport rates at the monitoring locations are determined with physical samples obtained with a TR-2 bedload sampler. These measurements are used to define quantitative relationships linking water flow and sediment discharge, which are then used to estimate total gravel loads transported past the monitoring locations during the annual flow releases (details on the sampling and analysis methods can be found in annual sediment monitoring reports issued by the contractor, e.g. GMA 2016b).

Three monitoring stations [Trinity River at Lewiston (TRAL), Trinity River above Grass Valley Creek (TRGVC), and Trinity River below Limekiln Gulch (TRLG)] are upstream from Indian Creek (Figure 1). TRAL, TRGVC, and TRLG are located 110.15, 104.85, and 98.9 River Miles upstream from the Klamath River confluence. These monitoring locations are critical for assessing where gravel augmentations have or have not altered gravel mobility and transport in the reaches where gravel supplies are actively managed. Gravel load estimates at these locations are valuable for corroborating load estimates determined by topographic differencing and validating morphology-based sediment budgets. They also support assessment of how transport rates are changing over time in response to upstream augmentations. One of these sediment monitoring locations, TRGVC, is of particular significance in this report, because it is located 500 ft downstream from the Lowden Ranch high-flow gravel injection point (Figure 5). Gravel loads estimated from transport at that location are used in this report as an internal boundary for a morphology-based gravel budget. The fourth monitoring location, Trinity River at Douglas City, is located downstream from Indian Creek (River Mile 92.7) and is most useful for assessing target transport rates for the more upstream monitoring locations (Gaeuman 2014b).

In addition to physical sediment samples, gravel transport rates in 2015 were also monitored at Lowden Ranch using experimental seismic and passive acoustic methods. Recent research suggests that coarse sediment transport generates acoustic and seismic vibrations that can be used to identify the onset of transport and quantify transport rates (Schmandt et al. 2013; Marineau et al. 2015). Seismic observations were collected in collaboration with a research team from the University of New Mexico, who deployed an array of seismometers spanning the Lowden Ranch reach during the 2015 flow release. The seismic array was composed of 76 cable-free 10-Hz geophones that record vertical ground motion at a sample rate of 250 Hz. An additional three-component broadband seismometer was installed in the middle of the array. Passive acoustic data were collected and analyzed by researchers from the US Geological Survey's California Water Science Center. The acoustic monitoring system consisted of a pair of hydrophones installed on either side of the river near the TRGVC sediment monitoring transect. Additional details on the instrumentation can be found in Marineau et al. (2015). Each hydrophone recorded 1-minute audio samples as 44.1 kHz, 16-bit stereo (2-channel) .wav files at 20-minute intervals over the flow release. Both of these surrogate technologies proved useful for corroborating the results of the conventional transport measurements and extrapolating those transport rates to the reach scale.

Uncertainty

Because of the very large numbers of individual point elevations (several to hundreds of points per yd^2) obtained by the sonar and LiDAR methods used to collect topographic data for this study, random errors associated with single elevation points have little meaning for assessing uncertainty margins when computing mean surface elevations because averaging over many points effectively eliminates their effect (Grams et al. 2013; Gaeuman 2014a). The potential for systematic errors that result in survey bias, however, is extremely important in that the resulting error increases linearly with the spatial extent of the survey. For example, a relative bias of +0.1 ft between a survey conducted at time 1 and another survey conducted at time 2 would produce a volumetric error of +3 yd^3 if the study area covered 90 yd^2. But that same bias would produce a volumetric error of +161 yd^3 if the survey were extended over an acre. Whether uncertainties of these magnitudes are acceptable will depend on the magnitude of the actual changes the surveys are intended to detect.

Relative bias is likely in situations where the survey equipment and the associated mounting apparatus is dismantled and reassembled or otherwise altered between the successive surveys. The contractor that collected the 2011 bathymetric data conducted bias tests by reassembling the sonar sweep system between repeated surveys of the same surface and concluded that survey-to-survey relative bias associated with that system is less than 0.04 ft (Gaeuman 2014a). The precision of the 2015 multibeam sonar surveys were assessed by comparing elevations obtain in successive surveys of a portion of the river bed with a bedrock substrate that was observed to remain essentially unchanged over the study period. This resulted in an estimate for the likely bias between repeated multibeam sonar surveys of 0.008 ft. Because the analyses that follow use elevations obtained with both of these methods, we summed the biases associated with each method to arrive at a net bias between the first and final surveys of ± 0.048 ft.

Errors can also arise from differences between the bulk densities of the gravel substrate versus stockpiled gravel used for gravel injections and in the conversion factor used to convert gravel loads determined from physical sediment sampling to substrate volume equivalents. Gaeuman (2014a) measured the bulk density of stockpiled gravel at 1.45 tons per yd^3 and used published data to estimate the typical density of the gravel component of gravel-bed river substrate of to be 1.61 tons per yd^3. These values are used below to convert stockpiled material and sampled gravel bedload to volumetric units that are comparable to the results of topographic differencing. All such conversions are assigned uncertainty margins of ± 10%. As these types of errors of independent of survey errors, they are combined with the survey uncertainties as the root sum of squares.

The potential for error in the bedload flux computed at TRGVC from physical samples represents another source of uncertainty in the gravel budget developed below for the Lowden Ranch site. Sediment sampling is subject to numerous types of errors, including failure to obtain a sufficient number of samples to adequately capture temporal and spatial variability in transport rates and logistical difficulties that limit the accuracy of the physical samples themselves. The impact of this type of uncertainty, as well as the effect of survey bias, is evaluated more thoroughly later in the context of the gravel budget results.

Surface Substrate Conditions

Initial Bed Surface Grain-size Monitoring by GMA

Bed surface grain-size monitoring began when Graham Matthews and Associates, a contractor working for the Program, obtained sets of substrate photographs at 55 sites between Lewiston Dam and Weaver Creek in October and November 2013 (GMA 2015). Sites were numbered sequentially in the downstream direction beginning with zero at the first site downstream from Lewiston Dam. The photo set collected at each site consisted of two to four adjacent downward looking images of the substrate in representative areas near the upstream ends of emergent bars. Photos were taken with a Canon EOS 5D Mark II digital camera attached to a horizontally-mounted tripod at the top of a 10-ft step ladder. This height above the substrate allows the camera field of view to encompass a sample area of about 60 ft^2, such that the set of adjacent photos covers an area of 120 to 240 ft^2. This is 150 to 300 times larger than the area of the largest particles present, so the samples exceed the 1% sampling criterion recommended by Church et al. (1987). Each photo was framed with stadia rods positioned around the perimeter of the field of view and included three to six tennis balls placed within the frame. A total of 167 substrate photos and 110 conventional photos showing the sample location were taken. All substrate images were corrected for lens distortion during post-processing with GNU Image Manipulation Program (GIMP). The location of each frame center was georeferenced with RTK or Differential GPS. Field pebble counts were obtained at the time and place of photo acquisition at sites 10, 20, 30, 41, and 45 using the heel-toe selection method (Wolman 1954) and a gravelometer (metal template) with square openings corresponding to ½-ϕ size classes, where ϕ is defined as the negative base-2 log of the opening diameter. Five additional pebble counts were performed at sites 0, 7, 22, 50, 55 in April 2014. Between 118 and 137 particles were sampled per site.

GMA performed an initial comparison between the field pebble counts and grain sizes measured on the substrate photographs as follows: A digital point grid was overlain on the photographs and scaled so that points would fall on and identify at least 150 individual particles for measurement at each site. The *b* (intermediate) axis of each identified particle was visually determined and measured with the measure tool in the GIMP software and binned into ½-ϕ classes. If the particle boundaries were obscured, the next particle up and to the left of the particle was selected for measurement.

The particle size distributions obtained from the photographs deviate substantially from the field-determined distributions. GMA reported differences between the field and photo-derived median grain sizes (D_{50}) of less than 10% at just three sites (Table 4). Three more sites had moderate discrepancies ranging from 18% to 32% in absolute error magnitude relative to field measurements. Two more sites had large absolute discrepancies of 65% and 79% in D_{50} values, and the final two sites showed extreme discrepancies of 116% and 146%. The photo-derived D_{50} values were larger than those derived from field measurements in all but two cases, the exceptions being the instances with the smallest discrepancies ($\leq$ 8%). GMA explained this difference by noting that stones with *b*-axes that exceed the dimensions of a square hole in the gravelometer can pass through diagonally if the stone's shortest (*c*) axis is relatively small. Discrepancies in pebble counts can also arise due to differences in how different individual pebble counts are performed (Wohl et al. 1996; Bunte and Abt

2001a). With an average absolute deviation magnitude of 50%, the differences were such that GMA suspended further analysis of the photographs and instead focused efforts on identifying the source of the discrepancies.

In October 2014, GMA revisited six of the original 55 locations (sites 2, 16, 18, 25, 47, 54) to conduct pebble counts using both a gravelometer and a ruler. Instead of the heel-toe sampling method, they placed a welded wire mesh on the bar surface to define a sampling grid with a horizontal spacing of 1 ft. Ruler measurements were used to define particle size statistics in two ways: one size distribution was computed from the measured *b* axis dimensions and a second distribution was computed by binning the ruler measurements into ½-ϕ size classes for direct comparison with the gravelometer results.

Ongoing Evaluation of Photographic Substrate Monitoring

We recently began to reevaluate the potential to document and monitor surface substrate conditions using advanced photogrammetric software to merge multiple ground-based photographs into a single high-resolution orthorectified image. This method eliminates the need to elevate the camera above the bar surface and greatly reduces the ground control required to accurately scale the images. It is therefore logistically simple and inexpensive to implement. We have also begun to investigate the feasibility of using image processing software to automatically extract grain size statistics from the substrate images. Use of such software has the potential to greatly speed the data reduction process by eliminating the need to sample and measure individual particles on the digital images.

The utility of both types of software was assessed with a pilot study conducted in the summer of 2016. Bar surface substrate characteristics were sampled at four sites along the Trinity River. From upstream to downstream, the sites are Steelbridge (RM 99.03), Riffle Lane (RM 94.69), Hidden Bar (RM 90.08), and Lillys Bar (RM 79.37). The Steelbridge and Riffle Lane sites correspond to GMA sites 46 and 58, respectively, whereas the other two sites are downstream from the reaches sampled by GMA.

Field Methods

We selected sampling areas where the substrate appeared to be undisturbed, spatially consistent, and free of vegetation on each of the four bars. Each sampling area was framed by a pair of extended stadia rods that defined a rectangle approximately 20 ft long and 12 ft wide. Colored whiffle balls were secured at three points just outside the sampling area with large nails driven through the ball and into the substrate. Information for scaling the images was obtained by measuring the distances between each pair of balls with a tape. Each sampling area was then photographed using a high-quality digital camera with a fixed focus lens. Rather than photographing separate frames as was done in 2013, we obtained large numbers of overlapping photographs. The photographer first walked around the perimeter of the sampling area, taking slightly oblique photographs spaced about 2 ft apart near the edge of the sample. The photographer then performed a series of lateral traverses across the sample, beginning at one end of the area and finishing at the other end, while continuing to collect closely-spaced photos of the substrate immediately ahead. In all, between 50 and 100

near-vertical photographs of the substrate were obtained at each site. This procedure was adopted to avoid disturbing the substrate prior to photographing it. At all times, field personnel took care to minimize surface disturbance that might bias the subsequent pebble count.

Pebble counts were performed by laying a tape parallel to the long dimension of the sampling area about one-sixth of the distance from one stadia rod to the other. Sampling proceeded by moving along the tape and measuring the *b* axis of whatever pebble lay exactly below each 1-ft tick mark on one edge of the tape. Measurements were performed with a ruler and recorded to the closest mm. After the sampling area was traversed in that manner, the tape was moved toward the far rod and the procedure for selecting and measuring pebbles was repeated. The tape was moved three additional times, resulting in a total of five equally-spaced tape traverses through the sampling area and about 120 measurements per site.

Data Reduction Methods

The set of overlapping photographs taken of each sampling area were assembled into a single orthorectified image using a photogrammetric method generically referred to as Structure-from-Motion (SfM). SfM is performed using software that implements autocorrelation and photogrammetric algorithms to construct 3-dimensional surface models from overlapping photographs. In this study, SfM processing was performed with Agisoft PhotoScan Professional. Images are loaded into PhotoScan, which aligns them and generates a sparse point cloud of tie points (points identified as being the same location in different photos) using autocorrelation routines. Camera calibration to account for and remove the effects of barrel distortion is performed using a subset of images taken of the same area with the camera rotated by 0, 90, and 270 degrees. We used the measured distances between the whiffle balls placed in the image area to define a coordinate system and scale for the point cloud, which is then used to generate a 3-dimensional mesh surface. That surface mesh can then be used to generate an orthorectified composite image, which we exported to JPG format for further analysis.

Surface grain size information was extracted from the orthorectified images of the sampling areas by manually measuring randomly sampled particles on the images. These photograph-based particles counts (PPC) were performed using ArcMap GIS software. Due to a peculiarity in how PhotoScan handles coordinates, the first step in this analysis was to reestablish a true scale in ArcMap by re-assigning the whiffle ball coordinates to those locations. A set of grids, each of which consists of approximately 120 randomly distributed points, was then generated by assigning each point in a regular grid a random number between zero and one and deleting all points with assigned numbers corresponding to arbitrary ranges of values.

Each substrate image was overlain with one of the randomized grids, and any substrate particles found to lie under a grid point was selected for measurement using the ArcMap measure tool. The identified particles were sometimes clearly visible in the photograph, such that the *b* axis could be easily measured. In addition to the diameter along the *b* axis of those particles, a measurement quality attribute of 1 was recorded. Many other identified particles,

however, were partially obscured by other particles or by shadows cast by other particles. In cases when enough of the particle boundary was visible to confidently identify the *b* axis and measure its approximate width, a measurement quality attribute of zero was assigned. Particles whose boundaries were mostly obscured and could not be identified with confidence were assigned a measurement quality attribute of -1. In those cases, the largest dimension of the visible portion of the particle was assumed to approximate the *b* axis dimension. In a very few cases (<10) where no part of the particle boundary was visible and no clues to the particle dimensions were apparent, the particle was omitted from the sample. The average quality scores computed for the four sampling sites ranged from -0.12 to 0.15, with an average across all sites of 0.02. These scores indicate that the measurements were typically performed on stones whose *b* axes could be identified with confidence.

Cumulative frequency distributions for the particle size measurements were computed separately for the field pebble counts and the PPC using raw measurements (no binning into size classes). These distributions define the fraction of the measurements that are equal to or greater than a given size. Expressed as percentiles, for example, the 50th percentile particle size (D_{50}) is equal to or larger than half of the particles in the sample and the 90th percentile size (D_{90}) is equal to or larger than 90 percent of the particles.

Another set of particle size percentiles was derived for the 2015 substrate samples using DGS, a Matlab script that analyzes the spectral characteristics of the image to automatically estimate particle size percentiles (Buscombe 2013). This script is publically available for download at https://github.com/dbuscombe-usgs/DGS. Orthorectified images are easily loaded into DGS using a prompt box that appears upon initialization of the script. The pixel size in millimeters, as defined in PhotoScan, is then entered, a region of interest is selected for analysis, and the analysis is executed. Results are displayed graphically and can be exported to CSV file containing a variety of statistics describing the derived particle size distribution, including the particle sizes corresponding to the 5th, 10th, 16th, 25th, 50th, 75th, 84th, 90th, and 95th percentiles.

Analyses and Results

Topographic Change at the Diversion Pool

Topographic changes at the Diversion Pool were assessed for the period between the summer of 2011 and the summer of 2015. Due to the relatively low flow and lack of gravel augmentations between 2011 and 2015, any topographic changes observed during that period are assumed to primarily reflect the effects of the 2015 flow release and the 2015 gravel injection. The 2015 elevation grid is displayed in Figure 7. The quality of the 2015 grid is considered to be excellent throughout its extent, but the same cannot be said of the 2011 terrain model, which lacks accurate bathymetry in large sections of channel near the Diversion Pool. Within the extent of the 2015 grid, the 2011 grid is reliable only in portions of the Diversion Pool itself, in the pools upstream and downstream from the New Lewiston Bridge, and in the floodplain area on the inside of the bend upstream from the bridge (outlined in black on Figure 7). Inspection of the 2011 terrain reveals that actual surveyed elevations (i.e., not interpolated) are almost entirely absent outside of those areas.

The results of topographic differencing are shown on Figure 8. Much of the differencing domain is characterized by small patches of erosion (blue) and aggradation (red/purple), but erosion appears to dominate. The average elevation change over the surveyed area is −0.052 ft for a net volume loss of 340 yd^3 of coarse bed material. This result is of limited significance because the lack of 2011 topographic data in much of the bend precludes the possibility of assessing changes in sediment storage at the reach-scale. Local patterns of erosion and aggradation, however, are more informative.

Aggradation is concentrated in three discrete locations: on the right side of the channel near the upstream end of the differencing domain, along the right edge of the wetted channel at the point of maximum channel curvature, and at the far downstream end of the differencing domain (Figure 8). Aside from those locations, the reach appears to be dominated by erosion. In particular, the bar and floodplain area on the interior of the bend shows a net decrease in coarse bed material volume of 540 yd^3, even when the band of aggradation at its outer edge, which accounts for a storage increase of 310 yd^3, is included. About 28% of the net erosion over the entire right-bank area (150 yd^3) is found in an elongated patch of erosion located slightly to the north-northwest of the previously mentioned band of aggradation. The effect of the erosion and aggradation observed in those areas was to equalize the elevations in those areas, as compared to their 2011 configuration. In 2011, the area corresponding to the band of erosion was mostly between 1818 and 1821 ft in elevation, whereas the area corresponding to the band of aggradation was mostly lower than 1817 ft. The 2015 flow release eroded the edge of the higher area and aggraded the lower area so that much of both areas were at about 1818 ft in elevation following the release (Figure 9).

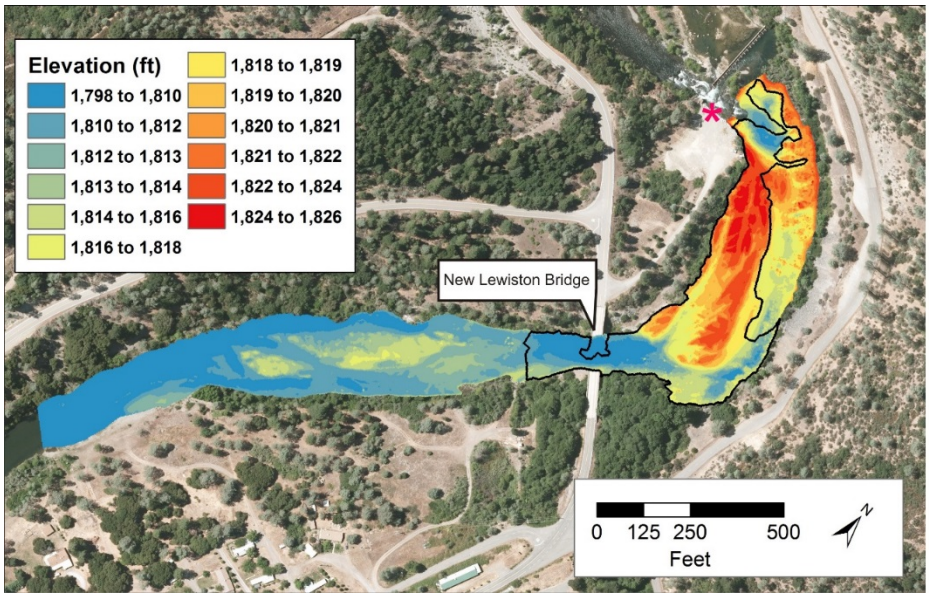

Figure 7: 2015 aerial photograph of the Diversion Pool reach showing the elevation grid developed from the 2015 survey data. The red asterisk indicates the gravel injection location. Flow is toward the left. Reliable elevation data from the 2011 terrain model overlaps the 2015 survey area only within the region outlined in black.

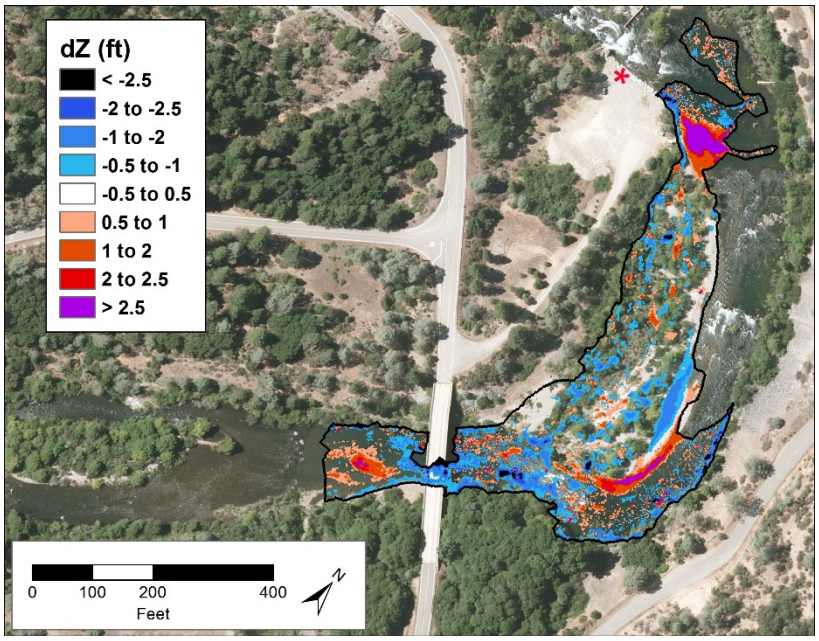

Figure 8: 2015 aerial photograph of the Diversion Pool reach showing elevation changes (dZ) between late 2011 and late 2015 after the spring flow release. The red asterisk indicates the gravel injection location.

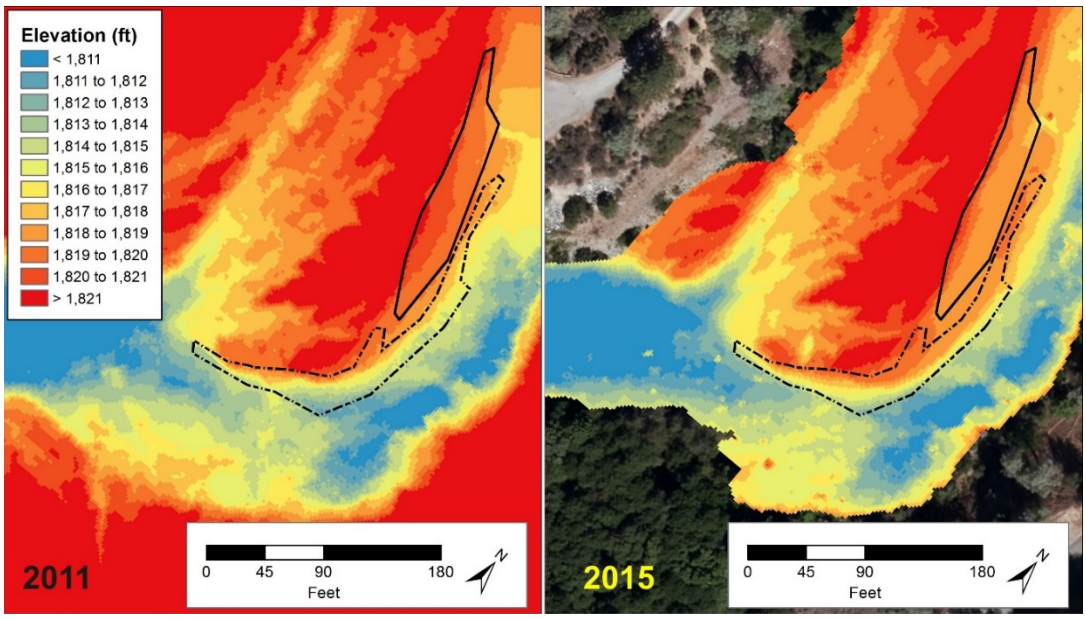

Figure 9: 2011 and 2015 topography at the apex of the bend downstream from the Diversion Pool. The locations of the band of erosion and aggradation shown on Figure 8 are indicated by the solid and dashed polygons, respectively.

Topographic Change at Lowden Ranch

The Lowden Ranch reach has been subject to a diverse set of management and monitoring actions over the past several years, beginning with the construction of the Lowden Ranch rehabilitation project in 2010 and a high-flow gravel injection performed at the downstream end of the site in the spring of that year. An as-built topographic survey was performed following project construction and a second high-quality topographic survey of the reach was performed after the 2011 flow release. According to Gaeuman (2014a), the combination of that 2011 flow release and gravel injection near the upstream end of the site resulted in bar growth, local pool scour, and a 36% increase in the standard deviation of bed elevations in the straight section of channel between the injection point and the islands at the downstream end of the site (location shown in Figure 5). Gaeuman (2014a) referred to that area as the Lowden Ranch target reach, because the 2011 gravel injection was intended to alter channel morphology in that part of the site.

Figure 10 depicts the changes in bed elevations observed between the 2011 survey and the first 2015 multibeam survey. That survey was conducted on the morning of May 5, about 20 hours after injection of about 306 yd^3 of gravel (adjusted to substrate bulk density) on the previous day and prior to the second injection. Two aggradation zones with maximum thicknesses exceeding 3 ft are evident – one at the upstream end of the surveyed area and another along the left bank just downstream from the injection point. Lesser amounts of aggradation (mostly between 0.5 to 1.5 ft) are visible near the center of the site, just downstream from two elongated zones of erosion where bed elevations decreased by as much as 2.7 ft. Taken together, the patches of erosion and aggradation downstream from the injection point suggest that the injected gravel deposited along the left bank, pushing the main stream flow toward the right bank where it caused local bed scour. The excavated material appears to have deposited a short distance downstream from its source area, forming low dune-like bedforms. Contrary to the significant geomorphic activity observed in the central and upstream portions of the surveyed area, bed elevation changes in the downstream third of the site rarely exceeded 0.35 ft.

Bed elevation changes observed between the successive multibeam surveys are shown in Figure 11. It is immediately apparent that elevation changes between the surveys following SBS1 were comparatively small, with the vast majority of the surveyed area showing bed elevation changes of less than 0.2 ft. Detectable geomorphic activity is mainly limited to the center of the site where a set of three to four bedforms appear to slowly migrate downstream over the remainder of the flow release. Downstream displacement of these small regions of scour and fill is readily apparent if the images in Figure 10 and Figure 11 are viewed as an animated sequence, but the motion is more difficult to perceive on still images. A pair of animations showing the evolution of bed elevations from 2011 through SBS4 are available on-line at http://trrp.net/perm/gaeuman/animation_approach_zone.avi and http://trrp.net/perm/gaeuman/animation_injection_zone.avi. The vertical dashed lines on Figure 11 are aligned with the leading edges of several small regions indicating local aggradation in the top image. Subsequent images show those small reddish regions moving past the vertical lines and being replaced in their original locations by blue regions indicating scour.

Figure 12 shows the total change in bed elevations over the full study period, i.e., from the summer of 2011 through the end of the 2015 flow release. The changes evident in Figure 12 are similar to those already noted for Figure 10 – aggradation is widespread at the upstream end of the surveyed area, along the left bank downstream from the injection point, and in the central part of the site downstream from a region of scour in the right half of the channel. Very little change is evident in the downstream third of the site or in the bend immediately upstream from the injection point.

To better examine these spatial differences in geomorphic response, we define four subreaches within the surveyed reach. The upstream quarter of the surveyed area is designated as the approach zone because it is the region in which incoming bedload transported from upstream approaches the Lowden project site (Figure 12). The next defined subreach is the bend immediately upstream from the gravel injection point. The channel through this part of the Lowden reach was straight prior to the 2010 rehabilitation project, which included excavation of the current bend and filling of the pre-project channel. The injection response zone is defined as the subreach downstream from the gravel injection point that responded to the 2015 gravel injection with substantial geomorphic change. Finally, the distal zone is defined as the downstream portion of the surveyed reach that showed little response to the 2015 gravel injection and flow release.

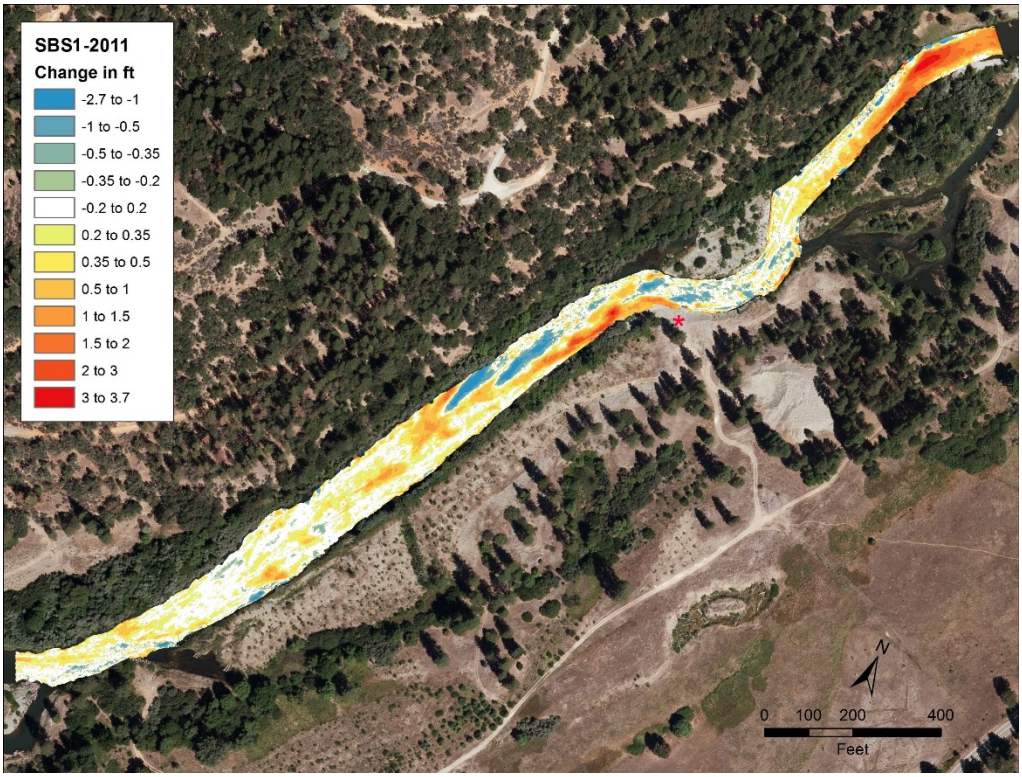

Figure 10: Bed elevation changes at Lowden Ranch between the summer 2011 sonar survey and the first 2015 multibeam sonar survey (morning of May 5). Injection point indicated with red asterisk.

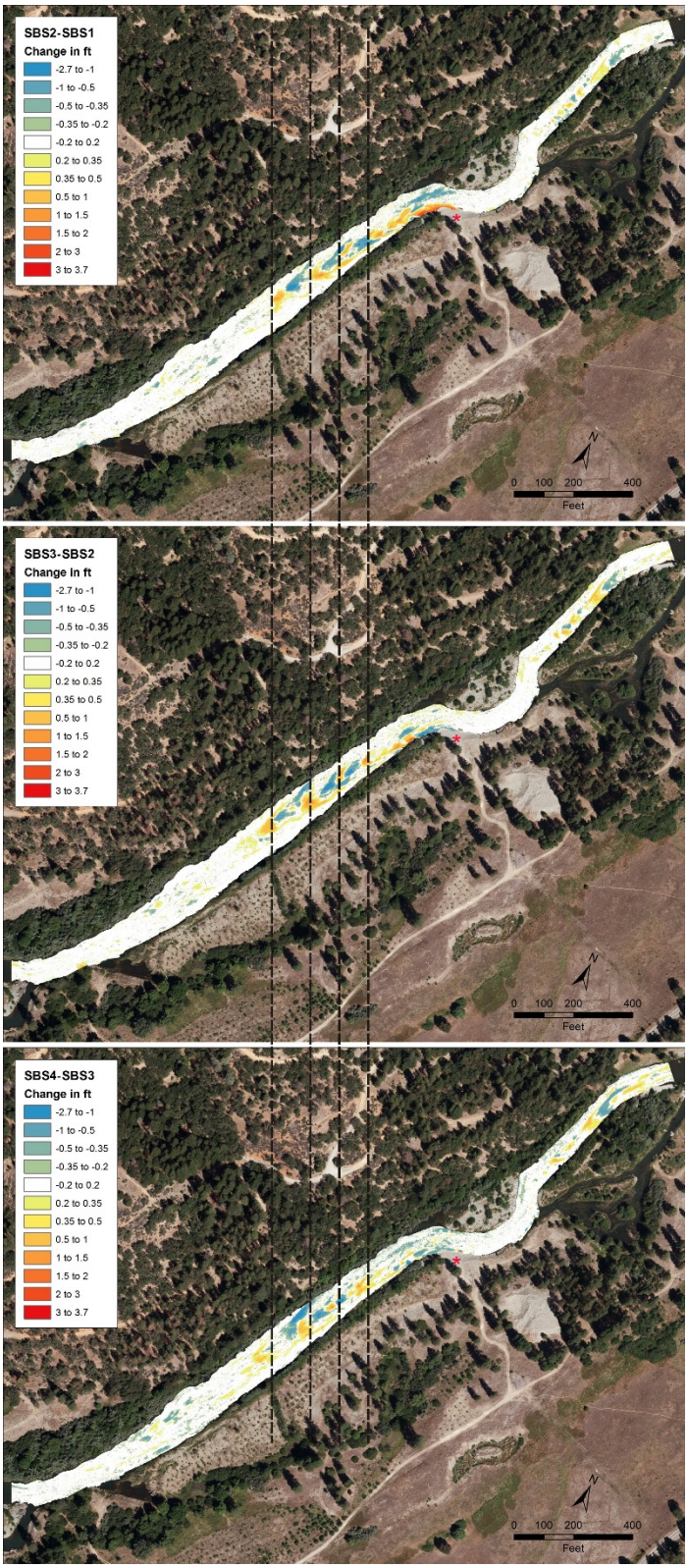

Figure 11: Bed elevation changes at Lowden Ranch between sequential multibeam surveys: SBS2 and SBS1 at top, SBS3 and SBS3 at center, SBS4 and SBS3 at bottom. Dotted lines are intended to provide a spatial reference.

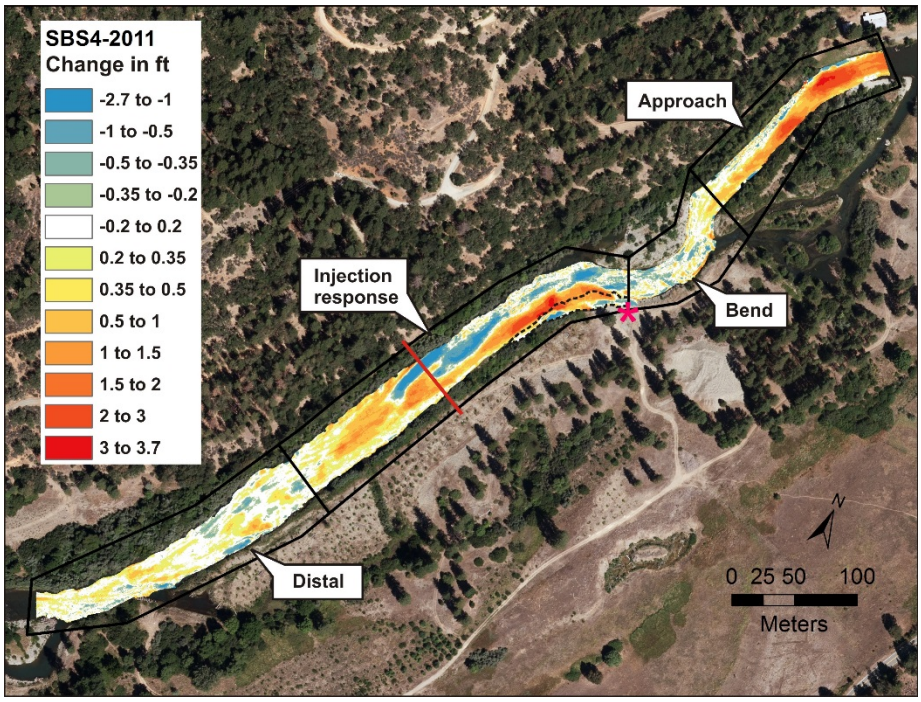

Figure 12: Bed elevation changes at Lowden Ranch between the summer 2011 sonar survey and the final 2015 multibeam survey (May 10). Sub-reaches with different types of geomorphic responses are indicated. The dashed line indicates the left bank area covered by conventional rod survey after the flow release.

The nature and timing of the geomorphic responses within the different zones are perhaps easier to observe when presented in profile view. For this purpose we defined three longitudinal profile lines through the Lowden site. One profile line was established in the center of the surveyed channel area, and two additional profile lines (one on each side) were established midway between the centerline and the edges of the channel area. Three sets of longitudinal profiles were then created by extracting bed elevations from each topographic dataset at 2-ft intervals along each of the three lines. The resulting profiles in each zone are discussed in order of upstream to downstream.

All three profiles through the approach zone indicate that virtually all of the aggradation observed in that zone occurred between the 2011 and the SBS1 surveys. Aggradation on the right approach profile takes the form of a smooth sediment wedge that locally approaches 3 ft in thickness, but is entirely restricted to the upstream third of the zone (Figure 13, bottom left panel). Aggradation on the center profile is also concentrated in the upstream half of the zone where it can exceed 2 ft in thickness some places, but aggradation in the form of small bedform averaging about 0.5 ft in height extends to the downstream end of the zone (Figure 13, middle left panel). The maximum aggradation of about 2 ft in thickness on the left profile is found in the center of the zone, where a single large dune-like form appears near station 225 on the SBS1 profile and migrates about 80 ft downstream over the remainder of the

release (Figure 13, top left panel). Aggradation thicknesses decrease toward both ends of the profile and nearly pinch out completely at the downstream end of the zone. Longitudinal profiles through the bend zone indicate very little change at any time during the study period. The largest changes in bed elevations are observed on the right profile line (Figure 13, bottom right panel), which displays slight aggradation and minor bedform development in its upstream half and areas of erosion farther downstream. Changes to the center and left profiles (Figure 13, middle and top right panels) are limited to minor aggradation within 100 ft of their upstream ends and development of ripple-like bedforms in a few isolated locations.

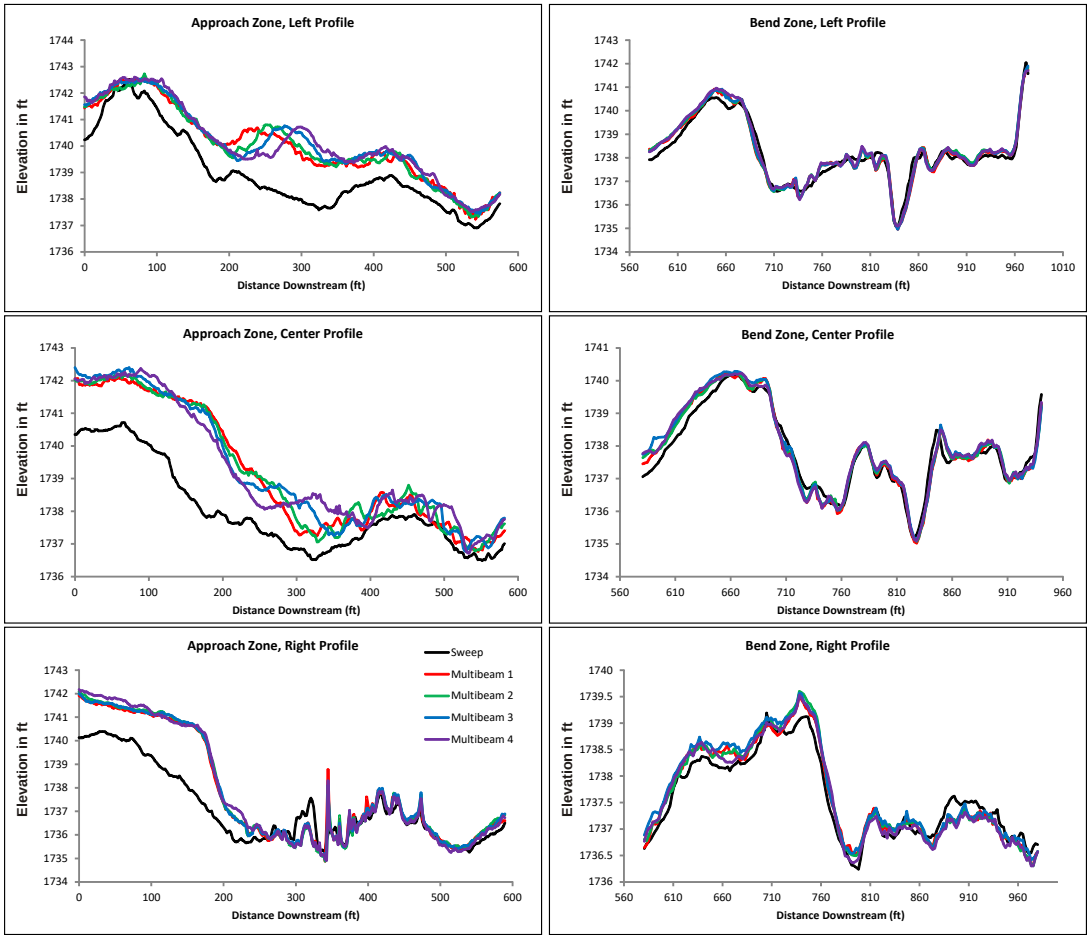

Figure 13: Bed elevation profiles through the Lowden Ranch approach zone (left) and the bend zone (right) at five points in time between summer 2011 and the end of the 2015 flow release.

Profiles through the injection response zone show areas of scour as well as regions with substantial aggradation. The left injection zone profile is characterized by widespread aggradation in the upstream two-thirds of the zone, primarily during the 2011-SBS1 and, to a lesser extent, the SBS1-SBS2 time intervals (Figure 14, top left panel). This profile traverses the tongue of aggradation visible on the left side of the channel immediately downstream

from the gravel injection point. Numerous small bedforms or other surface irregularities are present, but the relationship between the bedforms that appear on successive profile configurations is uncertain. It is clear, however, that the leading edge of the depositional region extended about 100 ft downstream from the sampling transect.

The center injection zone profile shows relatively little systematic change in its upstream third, but considerable scour and bedform activity farther downstream (Figure 14, middle left panel). The SBS1 profile shows that a broad dome-like structure present in the 2011 profile had been scoured to a depth of up to 2 ft approximately between stations 1300 and 1480, while two or three dune-like bedforms up to 1.5 ft high appear immediately downstream. Two of the dunes migrated 70 and 100 ft downstream over the remainder of the flow release, whereas a third dune-like form that appears near the downstream boundary of the zone in the SBS1 profile remained nearly stationary. Bed material approaching the downstream end of that profile after SBS1 apparently stalled about 100 ft upstream from the boundary of the zone or dispersed downstream.

The right injection zone profile is similar to the center one, in that its downstream end is more active than its upstream end (Figure 14, bottom left panel). The primary identifiable activity in the upstream half of the profile is the transfer of coarse bed material from a sharp topographic peak at about station 1050 to the base of the peak by the time of the SBS1 survey, and removal of the transferred material by the time of the SBS2 survey. At station 1520, however, the head of a large bar present in 2011 was scoured to a depth of at least 1.5 feet over a distance of about 100 ft by the time of the SBS1 survey, and a portion of the excavated material was deposited immediately downstream in the form of a dune about 1 ft high. As is the case in the center profile, this dune migrated as much as 100 feet downstream over the remainder of the flow release. In both cases, the most downstream dune on the SBS4 profiles appears to have grown in two-dimensional projected area (unit volume) compared to the corresponding dune on the earlier profiles. This suggests that a cross-channel sediment transfer, perhaps sourced from the tongue of injected gravel along the left bank, may have fed additional coarse bed material into the center of the channel toward the downstream end of the injection response zone. We investigated this possibility further by computing the net bed storage change between 2011 and SBS4 over a region that encompasses the dunes downstream from the sediment monitoring transect and the right half of the channel where net scour is indicated as far upstream as the gravel injection point, but excludes the tongue of aggradation along the left bank downstream from the injection point. Deposition in this region was found to exceed erosion by about 285 yd^3. This supports the hypothesis that some portion of the gravel, injected or otherwise, that was initially transported downstream along the left bank was transferred toward the center of the channel in the downstream half of the injection response zone.

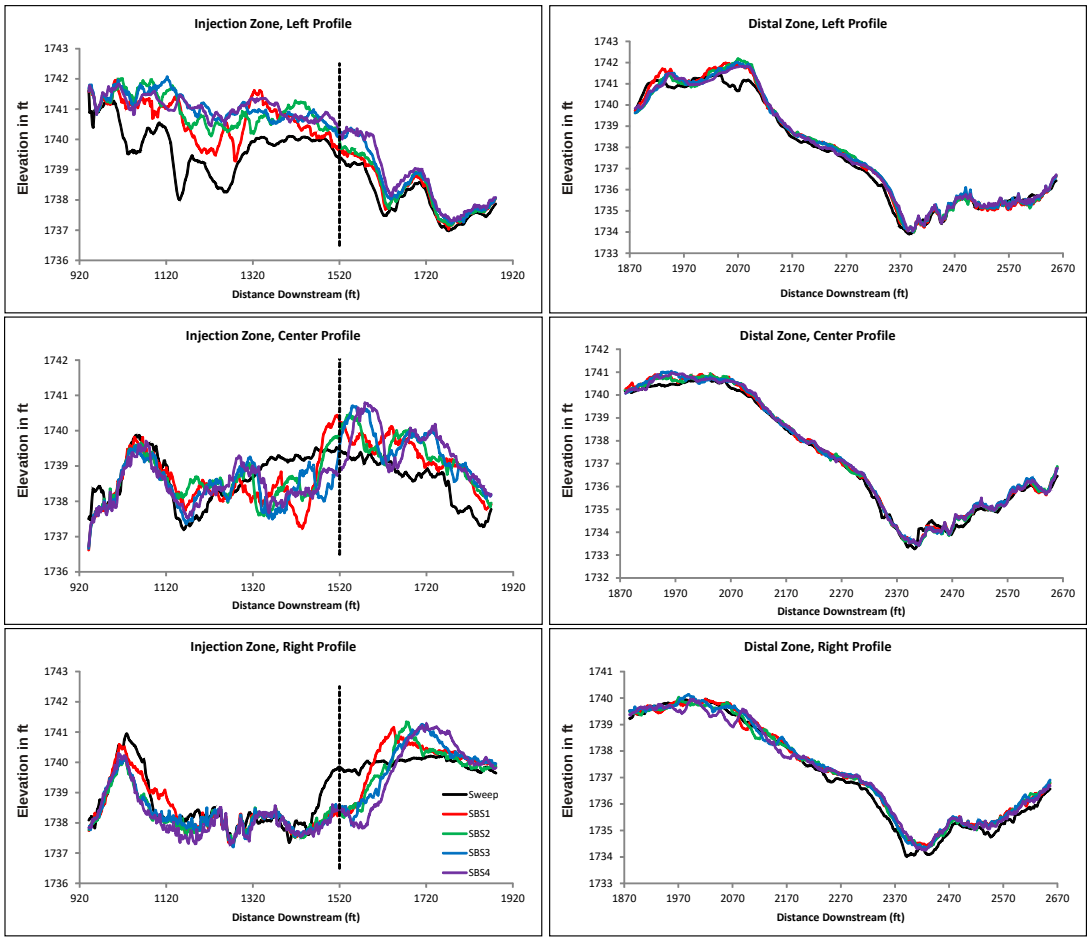

Figure 14: Bed elevation profiles through the Lowden Ranch injection response zone (left) and distal zone (right) at five points in time between summer 2011 and the end of the 2015 flow release. The vertical line indicates the position of the sediment monitoring transect.

Profiles through the distal zone also suggest that bed material fluxes decreased markedly downstream from the injection response zone. Comparing the left panels in Figure 14 with the right panels makes it clear that dunes propagating through the injection response zone did not continue into the distal zone. Instead, downstream transport essentially ceased, or changed from a process of bedform progradation to a dispersive process in which individual particles were transported entirely through the distal zone without interacting with the bed topography.

Rough indications of how much coarse sediment passed through the various zone and when the transport occurred can be obtained from a morphology-based sediment budget. For this analysis, we split the injection response zone into two parts – the upper injection response zone (IRZ1) is defined as the part of that zone lying upstream from the sediment monitoring transect and th lower injection response zone (IRZ2) is the part lying downstream from the sediment monitoring transect. This division allows for a comparison between the flux at that transect computed from bedload samples with a flux estimated from topographic changes. Table 2 tabulates changes in mean bed elevation (dZ) and bed material storage volume (dV)

computed for the different zones and time intervals. The left bank survey area was surveyed only once in 2015, after completion of the flow release. The total change in volume computed from that survey is reported in the SBS4-2011 column.

Table 2: Changes in mean bed elevations and bed material storage volumes determined from morphological differencing in subreaches of the the Lowden Ranch site. Uncertainty in dZ due to survey bias over the full study period is ± 0.048 ft in all zones.

	Area	SBS1-2011		SBS2-SBS1		SBS3-SBS2		SBS4-SBS3		SBS4-2011	
Zone	(yd^2)	dZ ft	dV yd^3	dZ ft	dV yd^3	dZ ft	dV yd^3	dZ ft	dV yd^3	dZ ft	dV yd^3
Approach	4422	0.832	1226	0.012	18	0.047	69	0.003	4	0.894	1318
Bend	2983	0.071	71	0.01	10	0.022	22	-0.045	-45	0.058	58
IRZ1	5845	0.202	394	0.040	78	-5E-3	-10	-0.052	-101	0.283	360
Left bank	1008									0.402	135
IRZ2	5946	0.287	569	0.022	44	0.074	147	-4E-3	-8	0.099	751
Distal	8751	0.136	397	-6E-3	-18	0.017	50	-0.048	-140	0.099	289

Converting the storage changes listed in Table 2 to budget-derived bed material fluxes requires an estimate of the flux across at least one internal or external boundary. As no information that is independent of the measured storage changes exists to assess fluxes entering or leaving the study area, the only viable boundary condition available is the gravel flux crossing the TRGVC bedload sampling transect. That flux was computed by the contractor to be 1370 tons (GMA 2016b), which is equivalent to 851 yd^3 using the conversion factor to substrate bulk density of 1.61 tons per yd^3. Bed-material fluxes in and out of the different zones computed using this boundary condition are tabulated in Table 3.

Table 3: Budget-derived bed material fluxes through the Lowden Ranch reach based on the assumption that the flux computed at TRGVC is accurate. dV listed for IRZ1 includes the left bank area. Renumber subsequent tables in document.

	Flux in (yd^3)	Injection in (yd^3)	dV (yd^3)	Flux out (yd^3)
Zone				
Approach	2722 ± 243	0	1318 ± 71	657 ± 179
Bend	1404 ± 179	0	58 ± 48	1347 ± 139
IRZ1 + left bank	1374 ± 139	612 ± 61	496 ± 110	851 ± 85
IRZ2	851 ± 85	0	751 ± 95	100 ± 128
Distal	100 ± 128	0	289 ± 140	–189 ± 250

It is immediately apparent that the fluxes listed in Table 3 cannot be strictly correct because a negative flux out of the distal zone is a physical impossibility. However, the uncertainty margin calculated for that downstream boundary is larger than the negative flux estimate, so that the budget indicates that the actual gravel flux out of the study area is most likely between zero and 61 yards. Overall, the budget implies that a relatively small portion of the gravel that entered the study area, whether from upstream or via injection, was transported as far downstream as the distal zone, and very little if any of it was transported past the downstream boundary of the distal zone. The budget also implies that virtually all of the bed

material that entered the bend zone (96%) was transport through the zone despite the fact that the associated change in storage is small and minimal change is apparent on topographic profiles through the zone (Figure 13).

These results are insensitive to exactly how the budget is adjusted to eliminate the original negative flux at the downstream boundary of the distal zone. Experimenting with potential values of survey bias shows that the negative boundary flux can be eliminated if it is assumed that the actual net bias between the first and final surveys is +0.039 ft (0.0119 m). Applying this assumption produces small decreases the estimated gravel inputs to the approach and bend zones of 7% and 9%, respectively. The negative flux can also be eliminated by assuming that the actual TRGVC load was 22% larger than originally reported. Numerous potential sources of error exist in the bedload flux computed from physical samples (Gomez et al. 1989; Gray et al. 2010), including random and systematic errors in the physical samples themselves, an insufficient number of samples to capture temporal variations in transport rates, or even the use of an imprecise factor for converting mass units to volume units. An error of 22% in the TRGVC boundary flux is therefore entirely possible. Applying that correction causes the inputs to the approach and bend zones to increase by 7% and 13%, respectively. If it is assumed that the two factors contribute equally and a bias correction of +0.019 ft (0.0058 m) is applied along with an 11% increase in the estimated TRGVC load, the computed inputs to the approach and bend zones remain close to the values shown in Table 3.

According to the gravel budget, the majority (96%) of the net change in gravel storage at Lowden Ranch occurred prior to survey SBS2 on the second day of the flow release peak. We believe that most, if not all, of that initial change occurred during the rise to the hydrograph peak on May 4 and or in the morning of May 5. Unfortunately, a sonar survey planned for the morning of May 4 was missed due to conflicting requests for data collection, so we lack topographic data to definitively confirm that belief. Several other lines of evidence, however, strongly suggest that very little geomorphic change took place between the summer 2011 survey and the beginning of the rise to the 2015 release peak.

As shown on Figure 2, flow releases to the Trinity River during the intervening years were generally too small to generate appreciable gravel transport on all but a few days. The discharge required for appreciable gravel transport indicated on that figure is based on years of bedload transport sampling in the Trinity River, including the 2015 samples from TRGVC plotted on Figure 3. Besides corroborating the assertion that gravel transport rates at TRGVC are very small when discharge drops below about 5000 ft^3/s, the 2015 sample data show that gravel transport rates on the rising limb of the hydrograph were often more than twice as great as rates measured after SBS1 despite the fact that the rising limb samples were collected when the discharge was just 80% of the peak value. The observed change in the discharge to gravel transport relation is consistent with the hypothesis that rate of geomorphic change in the reach had decreased substantially by the afternoon of May 5.

Finally, gravel loads computed from bedload samples collected in the preceding years also support the hypothesis that relatively little geomorphic change occurred in water years 2012 through 2014. The contractor who collects the bedload samples and computes loads based on

those samples reported annual gravel loads at TRGVC of 394 tons for 2012 and 39 tons for 2013 (GMA 2016b), whereas a gravel load of zero is assigned to the critically dry year of 2014. Thus, the load of 1370 tons reported for 2015 is 3.2 times as much as the total for the three previous years. In other words, approximately 76% of the total gravel transport between the end of the 2011 flow release and the end of the 2015 flow release occurred during the 2015 release. Comparing the sums of the positive changes in storage before and after SBS1 (Table 2) reveals that about 85% of all the topographic change detected in this study occurred prior to SBS1. Together, these considerations suggest that about 65% of the total geomorphic change incurred over the 4-year period between mid-May 2011 and mid-May 2015 was accomplished in about 20 hours.

Surrogate Gravel Transport Monitoring at Lowden Ranch

Seismic monitoring of coarse bedload during the 2015 flow release produced additional evidence that very little of the gravel that entered the Lowden Ranch site during the release was transported as far as the distal zone. Figure 15 shows the distribution of the 76 seismic nodes and single 3-component broadband instrument deployed for this study. After correcting the amplitudes of signals from the various instruments for distance from the river, the vertical component amplitude spectra from the broadband seismometer was used to identify signal frequencies between 20 and 100 Hz as having the strongest amplitude responses to the gravel injections (Schmandt et al. submitted; Gaeuman et al. 2016). Frequencies lower than 20 Hz were found to respond more closely with changes in water discharge. The time series of signals from each node were then filtered into different frequency bands for further analysis. Although data was collected continuously from early April through the mid-May, only data collected between 7 pm to 7 am were analyzed due to excessive seismic noise from traffic on nearby roads during the day.

The hourly mean amplitudes of signals in the 20–100 Hz range exhibited local maxima after each gravel injection followed by amplitude decay for 7 to 10 hours after the injections. The first episode of post- injection amplitude decay occurred during rising discharge and the second occurred during constant discharge so these transients are unambiguously linked to bedload rather than water transport (Figure 16).

The seismic nodes were separated according to whether they are within or near the injection response zone or the distal zone, as defined above for topographic analysis. Seismic waves from the river propagate in all directions so signals in the two zones are not entirely independent. However, signals with frequencies greater than 20 Hz were found to decay with distance by a factor of 10 or more over a distance of about 650 ft. Consequently, mean amplitudes within the injection response and distal zones are dominated by sources located within each zone. Both zones exhibited amplitude maxima following gravel injection, but the peak amplitudes following gravel injection were smaller in the distal zone than in the injection response zone and the durations of elevated seismic amplitudes were much smaller (Figure 16). The transient responses in the distal zone decayed to near baseline levels within a few hours following the gravel injections, whereas seismic amplitudes in the injection response zone remained at levels exceeding 75% of the maxima for days. Maps of signal amplitude at each node further illustrate the along-stream variation (Figure 17). The mean

signal amplitude in the injection response zone was 66% higher than in the distal zone, where very little topographic change was observed and the sediment budget indicates transport rates were low.

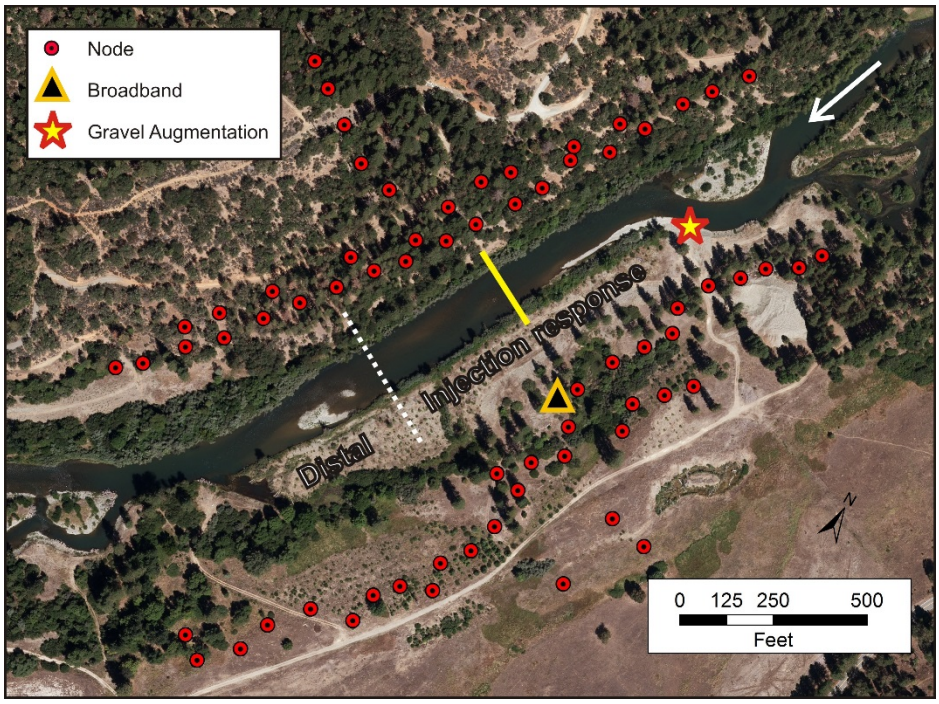

Figure 15: The locations of seismic nodes and the broadband seismometer within the Lowden Ranch site. The yellow line indicates the bedload sampling transect, the dashed white line is the boundary between the injection response and distal zones, and the white arrow shows the flow direction.

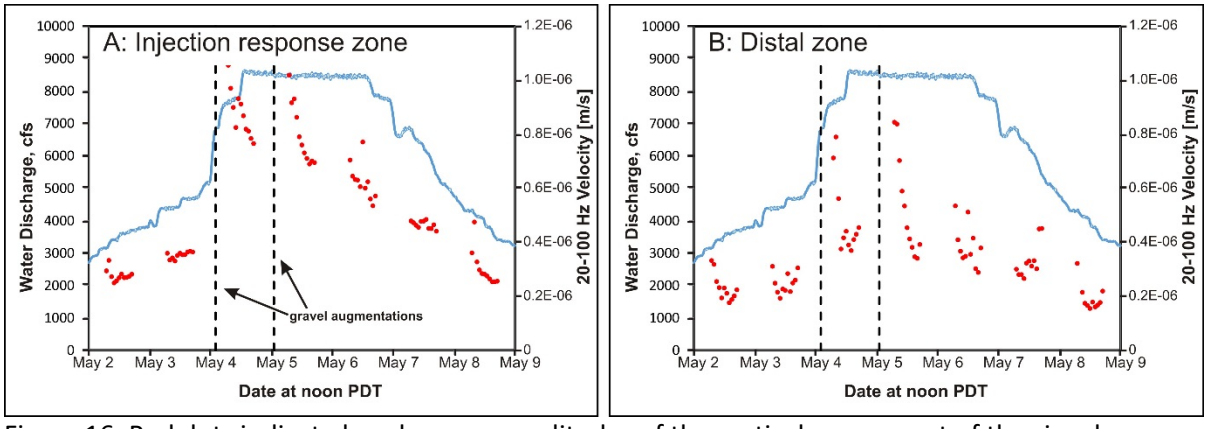

Figure 16: Red dots indicate hourly mean amplitudes of the vertical component of the signal between 20 to 100 Hz, averaged over A) the injection response zone and B) the distal zone. The flow release hydrograph is shown in blue.

In addition to providing evidence that gravel transport rates in the distal zone were substantially lower than in the injection response zone, the seismic results also lend support to the hypothesis that most of the gravel transport took place early in the hydrograph. A

steady decline in bedload generated seismic amplitudes over the peak flow period is clearly evident, particularly in the response zone where most of the transport occurred (Figure 16). This phenomenon can also be seen in acoustic signals recorded by hydrophones installed at the Lowden site. Marineau et al. (2016) found that sediment-generated noise (SGN) in the frequency range of 1 to 6 kHz correlated with gravel transport rates sampled at the Lowden Ranch site during the 2015 flow release better than did a rating curve based on discharge (r^2 = 0.88 for the SGN relationship versus r^2 = 0.79 for discharge). They developed a SGN-based gravel rating curve that, when applied to the time series of SGN recorded at the site, predicts gravel transport rates on the first day of the release peak and on portions of the rising limb that are 2 to 3 times greater than the rate predicted during the remainder of the release peak (Figure 18).

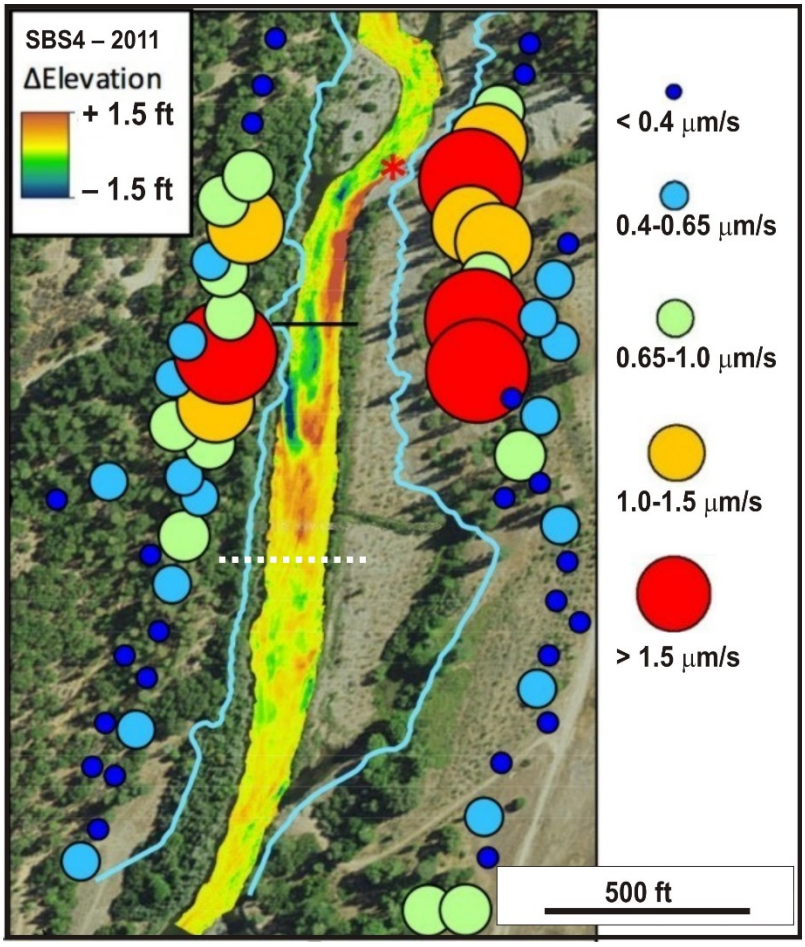

Figure 17: Spatial distributions of the mean hourly seismic amplitudes averaged over the three nights of highest discharge shown with topographic changes between the 2011 and SBS4 surveys. Symbol size and color correspond to nighttime median 20–100 Hz amplitude at each node. The dashed white line is the boundary between the injection response and distal zones, the black line is the bedload sampling transect and the red asterisk is the gravel injection location.

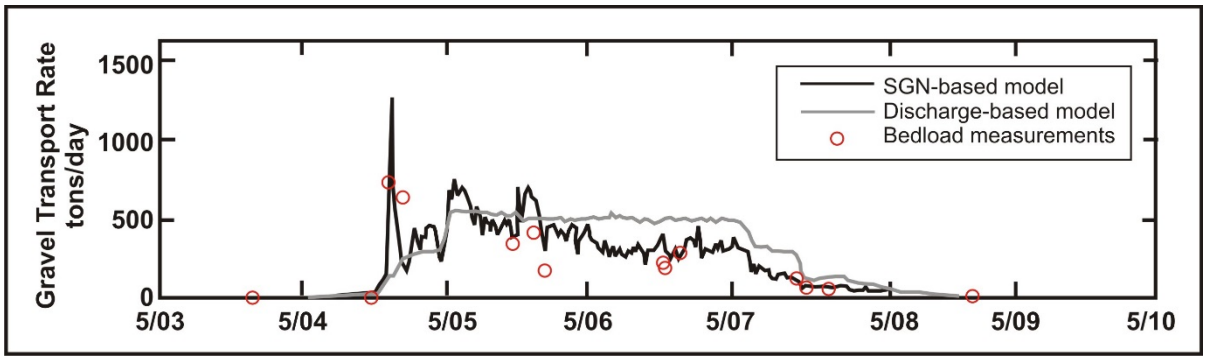

Figure 18: Time series of modeled gravel transport rates predicted at TRGVC using SGN (black line) and water discharge (grey line). Figure adapted from Marineau et al. (2016).

Surface Grain-size Monitoring

Initial Bed Surface Grain-size Monitoring by GMA

Comparisons between D_{50} values oobtained with the different methods showed that the gravelometer results were smaller (6% to 24%) than results obtained with binned ruler measurements at five of the six sites (Table 4). GMA excluded the 6th site visited in the fall of 2014 (site 18) from these analyses for reasons discussed below. Although the photo-derived D_{50} estimates at those five sites exceeds the 2014 gravelometer estimates, their average absolute deviation of 10% is much smaller than the average deviation from the 2013 gravelometer estimates. Conversely, the photo-derived D_{50} estimates for those five sites are all smaller than those obtained with field ruler measurements, with an identical average absolute discrepancy of 10%. Differences caused by binning or not binning the ruler measurements were considered negligible (1.7 mm on average).

GMA correctly pointed out that photo-derived measurements should be expected to produce somewhat smaller size statistics than a field pebble count conducted with a ruler for several reasons. First, the individual particles are rarely found in a perfectly horizontal position. Their *b* axis therefore appears smaller on a photograph than its true dimension, particularly in cases where the surface grains are strongly imbricated. Another factor that diminishes the apparent size of the particles is that portions of the individual particles are often obscured by other particles or shadows, such that only the exposed part of the particle is available for measurement. This visual sheltering effect also depends on the degree of particle imbrication and other attributes of bed surface is organization.

GMA appealed to these considerations to justify excluding the 6th site visited in the fall of 2014 (site 18) from analyses because its photo-derived D_{50} was 47% larger than that determined from the field ruler measurements (Table 4). According to GMA, this magnitude of positive error in the photo-derived measurements is extremely unlikely because all known mechanistic differences between field ruler measurements and photographic measurements produce negative errors. They indicated that the anomalous result for site 18 was due to an unidentified error of some kind. Although GMA did not explicitly consider it, we suggest that the bar surface at the site may have been altered between the fall of 2013 when the

photographs were taken and October 2014 when the pebble count was performed. Water year 2014 was a drought year in which the spring restoration flow release peaked near 1500 cfs, a flow that is well below the levels needed to mobilize the surface of gravel bars. In September of that year, however, a pulse flow that peaked at 3460 cfs was released from Lewiston Dam to help alleviate temperature and disease issues in the lower Klamath River. While that magnitude of flow is insufficient to generate widespread gravel transport in the Trinity River, it is almost certainly capable of producing localized changes to the bed surface.

Table 4: D_{50} values in mm for all sites visited and measurement methods used by GMA. Percent differences are photo measurement from field measurement. Where two differences are given, the gravelometer comparison is given first. Field ruler results are from binned measurements. Results for anomalous site 18 omitted from averages.

	River Mile	Field Gravelometer	Field Ruler	Photo Measure	% Difference
Fall 2013					
Site 0	111.60	26.9		48.3	79
Site 7	110.08	13.7		22.5	65
Site 10	109.46	25.5		24.9	–3
Site 20	106.75	66.0		83.6	27
Site 22	106.01	33.6		39.8	18
Site 30	104.26	70.0		64.4	–8
Site 41	100.27	62.9		82.9	32
Site 45	99.40	48.4		52.4	8
Site 50	97.99	25.4		54.9	116
Site 55	95.35	28.1		69.2	146
Average %difference					48
Average Abs(%difference)					50
Fall 2014					
Site 2	111.04	80.1	104	89.2	11/–14
Site 16	107.77	51.4	64.4	55.9	9/–13
Site 25	105.35	61.4	72.9	61.2	0/–16
Site 47	98.54	45.9	51.5	49.7	8/–3
Site 54	95.46	89.4	112	108	21/–4
Average %difference					10/–10
Average Abs(%difference)*					10/10

It is not surprising that the D_{50} values derived from photo-derived measurements correspond more closely with the field ruler results than with the 2013 gravelometer results. It is interesting, however, that the 2014 gravelometer results correspond much more closely to the photo-derived results than do the 2013 gravelometer results (10% discrepancies versus 50%). In fact, the 2014 gravelometer D_{50} values correspond with the photo-derived values as well as D_{50} measured by field ruler.

We see no obvious explanation for this apparent improvement in the gravelometer measurements, nor did GMA address it. Although the sampling protocol changed from a heel-toe method in 2013 to wire mesh grid in 2014, it is difficult to envision how this difference in methods could account for the observed difference in results. In our opinion, the heel-toe sampling method is likely to be biased toward the selection of larger grains, which would result in overestimation of the D_{50} values. A change to a less biased sampling method in 2014 should therefore have exacerbated the discrepancies observed in the 2013 data.

In conclusion, GMA indicated that pebble counts conducted on photographs of bar surfaces tends to underestimate the surface D_{50} determined by field pebble counts measured with a ruler by about 10%. They indicated that this level of deviation could be successfully accommodated by increasing the estimates by 10% to match a hypothetical field pebble count, or by simply comparing photo-derived estimates only with other photo-derived estimates. They also implied that the use of gravelometers should be avoided, because the errors associated with them depends on particles shape factor that can vary between locations.

Ongoing Evaluation of Photographic Substrate Monitoring

Cumulative grain-size distributions determined from field pebble counts, PPC, and the DGS computer script for each sample site are plotted in Figure 19. Plots for particle count methods consists of about 120 points each (the number of particles sampled), whereas the DGS plots consist of just nine points corresponding to the percentiles output by the software.

The distributions derived from PPC lie close to the field-determined distribution at three of the four sites. Two-sample Kolmogorov-Smirnov tests (Ross 2004) performed on the paired PPC and field-determined particle-size distributions at Riffle Lane, Hidden Bar, and Lillys Bar support the hypothesis that the sample pairs were drawn from the same distributions at the 99%, 99%, and 85% confidence levels, respectively. The PPC distributions deviates meaningfully from the field results only at Steelbridge, where the maximum deviation of nearly 0.15 between the cumulative frequency curves occurs at approximately the 55 mm. A two-sample Kolmogorov-Smirnov test performed for that site indicates that such a large difference between samples drawn from the same distribution would be expected just 18% of the time. The DGS result, however, show large deviations from the field results at all sites. In most instances, the DGS plot underestimates particles sizes over most of the percentile range and overestimates the size of particles larger than about the 80th percentile. The closest fit between the DGS and field distributions occurs at Hidden Bar where DGS provides a good match to the field result through about the 65th percentile, but greatly overestimates the sizes of larger particles.

Considerably more information is embedded in a grain-size distribution than is typically used in practice. For most applications it is sufficient to describe substrate characteristics in terms of a few summary statistics. We therefore quantitatively assess the degree of agreement between the field and the image-based measurements in terms of the D_{50}, the geometric mean grain size (D_g), and the geometric standard deviation (σ_g). D_{50} is the perhaps the most commonly-used metric for characterizing particle size in fluvial geomorphology and

sediment transport applications, although D_g is favored by some authors (e.g. Parker 1990). Several options are available for expressing the spread of particle size distributions about their mean or median values, but σ_g is chosen for that purpose here because it is consistent with the use of D_g. The geometric statistics are also appropriate for data that approximate a logarithmic distribution, such as is frequently assumed for sediment particle sizes.

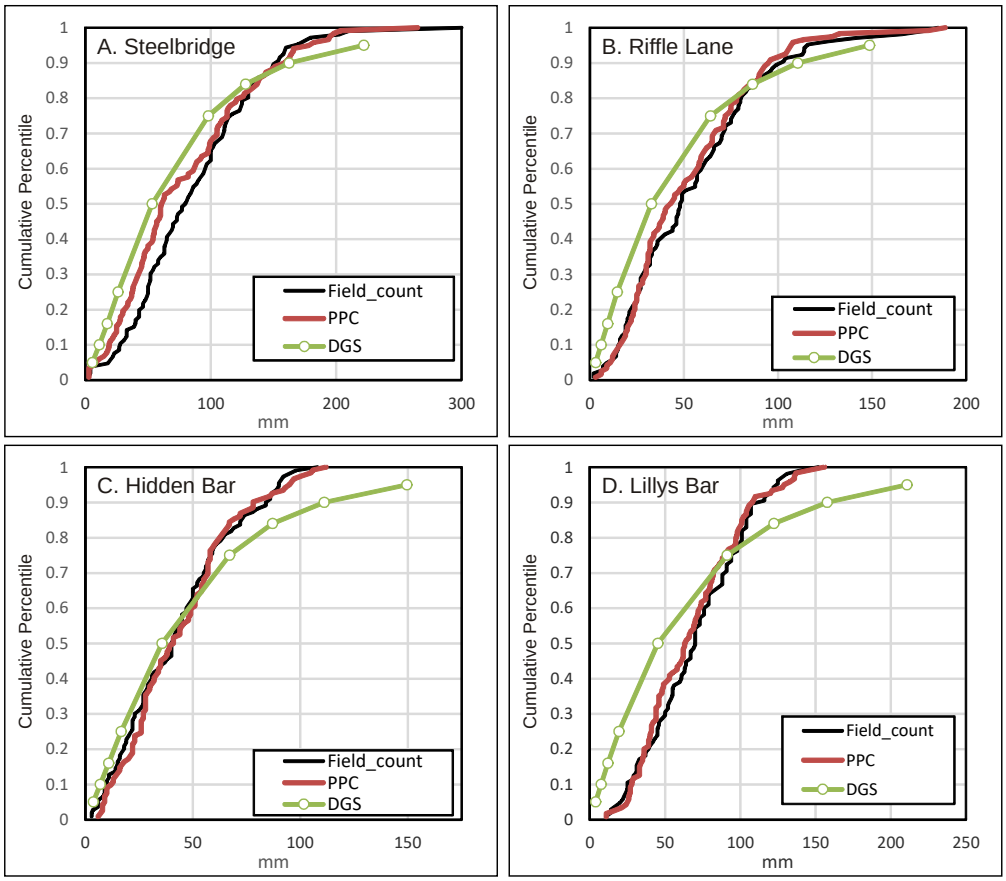

Figure 19: Cumulative grain-size distribution plots of the three measurement methods at each of the four locations sampled in 2016.

Computation of D_{50}, or any other percentile, is a simple matter – percentiles can be picked from sorted lists of measured data, and percentiles for DGS are found in the script's output file. The most straight-forward method for computing D_g is to multiply all n measurements in a dataset together and take the n^{th} root of that product. However, the DGS dataset consists of nine size percentiles only, so a method that makes use of the fractions of the data that fall in defined size classes is needed. The computation is:

$$D_g = exp(\sum f_i \ln D_i) \qquad (3)$$

where D_i is the representative diameter of grain size class i, f_i is the fraction of the distribution in that class. Although more information for computing D_g is available for the field and image-based pebble counts, all values of D_g were computed with equation (3) to ensure consistency across datasets. As a check, we compared D_g computed with equation (3)

with D_g computed from the complete sets of individual particle measurements and found them to be in good agreement. For the field measurements the average deviation is 1.2% and for the PPC measurements the average deviation is 0.6%. But values of D_g computed with equation (3) differed somewhat from geometric means reported in the DGS output files. In all cases, our estimates of D_g computed from the DGS percentiles are about 4% larger than the values of D_g computed within DGS. Comment lines within the DGS script indicate that the script computes D_g with equation (3), but we were unable to determine why the DGS results differed from our calculations.

Also for consistency among measurement methods, σ_g was computed for all datasets using grain size percentiles rather than the complete sets of measurements. In this case the equation is:

$$\sigma_g = exp\left[\left(\sum \ln f_i\left(D_i/D_g\right)^2\right)^{0.5}\right] \qquad (4)$$

As computed with equation (4), σ_g is a dimensionless number that quantifies the ratio of the standard deviation to the mean such that a uniform sediment (zero spread) has $\sigma_g = 1$.

The DGS script outputs a statistic it designates as the geometric standard deviation that is more properly identified as a dimensional version of the Folk and Ward (1957) sorting coefficient (Bunte and Abt 2001b). Comment lines within the DGS script indicate that it is computed as:

$$\sigma_{DGS} = exp\left[\frac{(\ln D_{84} - \ln D_{16})}{4} + \frac{(\ln D_{95} - \ln D_5)}{6.6}\right] \qquad (5)$$

Equation (5) yields the geometric standard deviation in units of length, provided the particle size distribution is log-normal. We chose to use equation (4) rather than (5) to compare measurement methods herein because we were unable to reproduce the values of σ_{DGS} reported in the DGS output files.

Table 5 lists the three metrics discussed above for the various sites and measurement methods. As expected, both types of image-derived methods tend to under-predict the D_{50} of the field-based distributions. Image-based particle counts, however, produce much smaller deviations than the automated method. D_{50} values obtained from PPC deviate from the field measurements by between –24% to +2%, whereas the deviations for DGS D_{50} values range from –10% to –36%. At 28%, the average absolute deviation in D_{50} obtained from DGS is more than twice that obtained from PPC (12%).

Similar results were obtained for values of D_g and σ_g. Values of D_g obtained via PPC deviate from the field results by –20% to +9%, with an average absolute deviation of 9%. At 27%, the average absolute deviation of D_gs values obtained from DGS is 3 times as large, with individual estimates ranging from –6% to –36%. Because all of the DGS deviations are negative, whereas the PPC deviations include a positive value, the average signed deviation for DGS is nearly 7 times as large as the signed PPC deviation (4%). Deviations in σ_g computed from the PPC measurements were relatively small, with an average absolute

deviation of 12% and a signed average of just +2% (Table 5). Values of σ_g computed from the DGS percentiles, however, range from +29% to +80% for average signed and absolute deviations of 50%.

Table 5: Grain-size distribution statistics for all sites visited and measurement methods used in 2016. D_{50} and D_g are given in mm; σ_g is dimensionless.

	Field	PPC	DGS
D_{50}			
Steelbridge	80	61	53
Riffle Lane	48	43	33
Hidden Bar	40	41	36
Lillys Bar	70	63	45
% difference D_{50}			
Steelbridge		−24	−34
Riffle Lane		−10	−31
Hidden Bar		+2	−10
Lillys Bar		−10	−36
Average % difference D_{50}		−10	−28
Average Abs(% difference) D_{50}		12	28
D_g			
Steelbridge	72.2	57.8	47.4
Riffle Lane	42.7	41.1	28.7
Hidden Bar	33.2	36.1	31.2
Lillys Bar	61.3	59.8	39.1
% difference D_g			
Steelbridge		−20	−34
Riffle Lane		−3	−33
Hidden Bar		+9	−6
Lillys Bar		−2	−36
Average % difference D_g		−4	−27
Average Abs(% difference) D_g		9	27
σ_g			
Steelbridge	1.86	2.37	2.73
Riffle Lane	2.05	1.96	2.96
Hidden Bar	2.18	1.95	2.81
Lillys Bar	1.72	1.65	3.09
% difference σ_g			
Steelbridge		+27	+47
Riffle Lane		−4	+44
Hidden Bar		−11	+29
Lillys Bar		−4	+80
Average % difference σ_g		+2	+50
Average Abs(% difference) σ_g		12	50

Discussion

Topographic Changes

The patterns of erosion and deposition observed on the right-bank bar and floodplain surface downstream from the Diversion Pool (Figure 8; Figure 9) are of interest because earlier analyses indicate that much, if not most, of the gravel injected at the Diversion Pool through 2011 had been sequestered in that area (Gaeuman 2011, Gaeuman and Krause 2013). In particular, high gravel ridges appeared along the margin of that area following the 2011 flow release. These ridges appeared to reach elevations approaching the water surface elevation associated with flows of 11000 to 12000 ft^3/s, raising doubts as to whether large flow releases are effective for routing gravel downstream. Instead, the evidence suggested that large flows have the potential to strand gravel in locations that more ordinary flow releases are incapable of accessing. The results presented here indicate that the moderately large flow release of 2015 was sufficient to produce erosion over much of the floodplain and remove portions of the highest part of the surface, evidently via lateral scour along their edges. These results also show that, as of 2015, gravel is routing through the bend and has moved at least as far downstream as the pool tailout between the New Lewiston Bridge and the island complex just downstream. Given that good topographic data now exists for the entire reach, the 2016 terrain model that is currently under development will likely make it possible to track the propagation of gravel through the Lewiston area.

Sediment monitoring data show that the total gravel load since 2004 at TRAL is 20% to 30% higher than at TRGVC or TRLG, which are the next two monitoring locations downstream (Figure 1). It cannot be determined, however, whether gravel injections at the Diversion Pool have contributed to the elevated bedload transport rates at TRAL because a total of about 7400 yd^3 of additional gravel was added between 2004 and 2009 at a location referred to as the Cableway, located 0.2 miles upstream from TRAL (Gaeuman 2014b). As of 2015, a total of about 13370 yd^3 of gravel had passed TRAL since 2004 (Gaeuman and Stewart 2017). Although this total is 1.8 times the quantity placed in the Cableway reach, there is no direct evidence that the Diversion Pool injections account for any portion of the excess. Regardless of whether gravel injected at the Diversion Pool reaches TRAL, we suspect that none of it (nor any of the gravel placed in the Cableway reach) has passed beyond the head of Cemetery side channel, located about 0.4 miles downstream from TRAL. This hypothesis is based on the observations that the area near that side channel bifurcation consists of a wide depositional riffle composed of relatively small gravel and on hydraulic modeling that indicates unit stream power and bedload transport capacities drop to very low levels at that location (Gaeuman 2014b). It may be possible to assess the validity of this hypothesis after the 2016 topographic model becomes available.

The 2015 sediment budget for the Lowden Ranch reach is consistent with earlier studies showing that ordinary flood events rarely move gravel more than a few to several channel widths downstream (Gaeuman 2011; Gaeuman and Krause 2013). According to the unadjusted gravel budget (Table 3), only about 13% of the 1273 yd^3 of gravel that entered the injection response zone was transported more than 1000 ft downstream and virtually none of it exited the Lowden Ranch site. Instead, that material was either deposited along the left

margin of the channel immediately downstream from the injection point, or was incorporated into a sequence of gravel dunes that formed on or just prior to the first day of the flow release peak and migrated between 80 and 100 ft farther downstream during the remainder of the release. Very little topographic change was observed in the distal zone downstream from where the advancing dunes ultimately stalled.

As in the distal zone, virtually no topographic change was observed during the flow release in the bend zone immediately upstream from the gravel injection point. But unlike the situation in the distal zone, the sediment budget indicates that a relatively large volume of gravel (equivalent to 87% of the injected gravel volume) passed through the bend zone. Thus, the absence of topographic change near the downstream end of the Lowden Ranch reach during the release appears to be the result of insufficient bed material delivered from upstream, whereas the absence of topographic change in the bend upstream from the injection point appears to be due to efficient throughput of bed material over a stable bed.

Finally, the approach zone at the upstream end of the Lowden Ranch site was geomorphically active during the 2015 release. According to the sediment budget, the gravel storage in that zone increased by 1318 yd^3 over the study period. This increase indicates that a large share of the bed material being delivered to Lowden Ranch from upstream is sequestered in the approach zone. Gaeuman (2014a) hypothesized that gravel entering the Lowden Ranch site during the 2011 flow release was captured in a backwater area corresponding to the approach zone defined herein. It was suggested that backwater conditions were present during the 2011 flow release due to channel realignment performed as part of the 2010 Lowden Ranch channel rehabilitation project. The current gravel budget suggest that this hypothesis may have been correct, but it also suggests that the area may have begun to approach its sediment storage capacity. Of the 1969 yd^3 of gravel estimated to have entered the approach zone since 2011 (Table 3), about one-third (651 yd^3) continued into the bend downstream.

As elsewhere in the study area, most of the storage change in the approach zone (93%) took place between the 2011 survey and the SBS1 survey. Given that about 76% of the total gravel load since 2011 was transported in 2015, about 71% of the total storage increase detected in the approach zone occurred during the 2015 release prior to the SBS1 survey. Over the full Lowden Ranch site, we estimate that 85% of the gravel transport and topographic change accomplished during the 2015 release and 65% of all the geomorphic work realized over the previous 4 years was achieved in about 20 hours on the rise and first day of the 2015 peak.

Despite the relatively short gravel transport distances indicated for Lowden Ranch by the 2015 data, it should be remembered that much greater transport distances can be attained in years with especially large flow events. Two such events have occurred in the last decade, one being the 2011 flow release in which the maximum daily mean flow at Lewiston reached 11600 ft^3/s and an estimated 2213 yd^3 of gravel (slightly more than was injected upstream) passed a boundary corresponding to the downstream end of the distal zone. The other event in which gravel was likely transported relatively long distances was the spring high-flow period in the extremely wet year of 2006 when the maximum daily mean flow release

reached 10100 ft^3/s and releases from Lewiston Dam were greater than above 6000 ft^3/s for 20 days. No information regarding gravel travel distance is available for that year, but the gravel load computed from sediment samples collected that year at TRGVC is more than three times the 2015 load.

Surface Substrate Monitoring

Three sets of data comparing metrics of particle size distributions obtained from field pebble counts and photography-based methods are discussed above. The first dataset, consisting of pebble counts collected by GMA in the fall of 2013 and subsequent analyses of substrate photographs, suggests that the photographic method employed can overestimate D_{50} values by close to 150% and produce average errors of around 50%. Errors of this magnitude imply that photography-based measurements may be of little value for substrate monitoring. However, much of the error in this initial assessment may be due to the use of several non-optimal sampling and measurement protocols. The 2013 field pebble counts were conducted using a gravelometer rather than a ruler to measure the sampled particles and an imprecise heel-toe sampling procedure that may promote undersampling of smaller particles. The sampling procedure used for selecting particles to measure on photographs is also somewhat suspect. Particles that were deemed to be obscured by other particles were replaced by selecting a nearby particle. It is possible that this sampling protocol leads to a bias toward the selection of larger particles on the photographs.

The two remaining datasets indicate that photography-based pebble counts tend to underestimate D_{50} values by about 12%. The improvement over the 2013 data can likely be attributed to improvements in the field sampling protocols. Field pebble counts used for these later comparisons were conducted using a ruler to measure the sampled particles and particles were selected for measurement using a physical grid (wire mesh or tape). The five pebble counts collected by GMA in 2014 indicate that errors associated with measuring particles on photographs are often near –15%. These photographic measurements were done using the same procedure for selecting alternate particles when sampled particles were obscured as was used for the 2013 data. Although the four sites we sampled in 2016 also displayed a negative bias in D_{50} values derived from counts on photographs, the estimates for three of those sites showed errors of –10% or less. This apparent decrease in the magnitude of negative bias relative to the 2014 GMA results could be related to a difference in how obscured particles on the photographs were handled.

We assessed D_g as an alternative measure of central tendency and found slightly better results (absolute average error = 9% and signed average error = 2%), raising the possibility that D_g is less prone to underestimation bias than is D_{50}. Our 2016 work also included an assessment of whether pebble counts on photographs can be used to accurately estimate the spread of the grain-size distribution, as quantified by σ_g. The precision of σ_g estimated from photographic pebble count appears to be similar to that observed for central tendency, with absolute errors averaging 12%.

Errors in D_{50} and D_g based on the output of DGS were more than twice as large as the errors associated with manual counts on photographs. In addition, DGS-based estimates of σ_g are at

least 4 times larger than those obtained from the manual counts. The magnitude of the errors in σ_g raises doubts as to whether the algorithms encoded in the script are capable of distinguishing between different particle size distributions. These doubts intensified by observing that the DGS distributions plotted Figure 19 are qualitatively similar, in that they all tend to underestimate the sizes of particles in the lower two-thirds of the distribution and overestimate the sizes of particles in the largest third of the distribution.

This apparent similarity in the nature of DGS errors between sites can be better evaluated by plotting the four particle size distributions for each of the three measurement methods on the same graph. This comparison is shown in Figure 20, on which particle size distributions for each method have been scaled to a common D_{50} to highlight differences in the distribution shapes. The plots of distributions based on field pebble counts and counts on photographs have been simplified to show only the nine particle size percentiles output by DGS for consistency with the DGS plots. The shape of the curves corresponding to the field pebble count results vary from site to site. For example, particles that are smaller than the median are slightly coarser at Lillys Bar than at the other sites, and particles larger than the median at that location are significantly finer than at the other sites (Figure 20a). Differences in the shapes of the curves at different sites are also evident in the curves corresponding to the manual counts on photographs, although the details of the differences are somewhat different than for the field data (Figure 20b). The curves corresponding to the DGS results, however, are strikingly similar from site to site (Figure 20c). The number of trials presented here are inadequate to draw any firm conclusions, but these result suggest that the particle size distributions output by DGS are severely limited in the shapes they can assume.

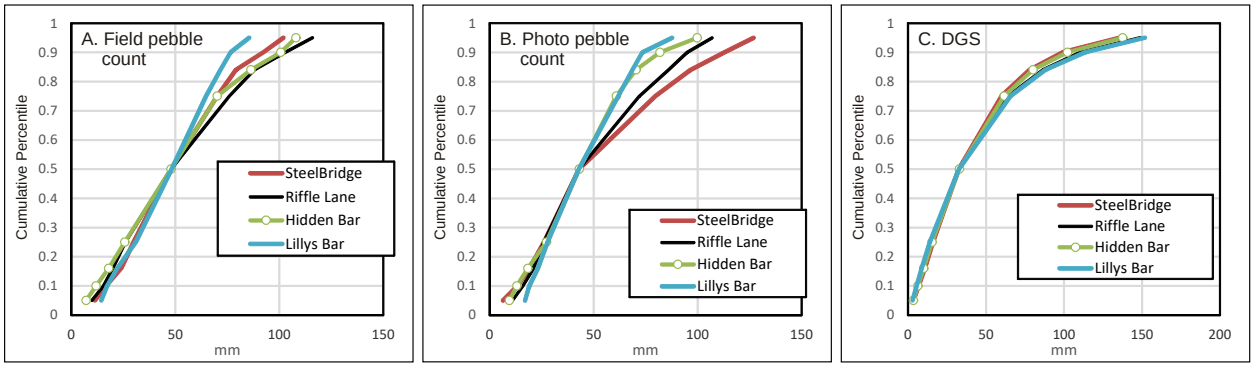

Figure 20: Scaled cumulative grain-size distributions at the four sampling locations plotted for each of the three measurement methods.

Conclusions

Previous studies have indicated that, as of 2012, most of the gravel injected at the Diversion Pool since 2008 was stored on the inside of a bend between 250 and 900 ft downstream from the injection point. The 2015 topographic data, however, provide the first clear evidence that gravel stored in that region has remobilized and propagated into the next reach downstream.

Repeat topographic surveys at the Lowden Ranch site combined with sediment monitoring results indicate that virtually all of the 680 yd^3 of gravel injected at that site during the 2015 flow release, as well as all the gravel delivered to the injection point from upstream, was deposited within about 1000 ft of the injection. Roughly half of that material deposited in the form of a lateral bar along the left bank immediately downstream from the injection, and the other half was deposited in the form of a series of gravel dunes. These dunes formed early in the flow release and subsequently migrated about one channel width downstream. About 85% of the geomorphic change occurred on the rise and first half day of the release peak. Relatively little change occurred over the remaining 2 days of the peak and the falling limb of the hydrograph.

Some portions of the Lowden Ranch site experienced substantial topographic change during the flow release, whereas bed elevations in other portions of the site remained constant. The gravel flux through one of the areas with stable bed elevations was small, but the flux through the other stable area was relatively large. The latter result underscores the fact that a lack of topographic change in a stream reach should not be regarded as evidence that the supply of bed material to the reach is deficient.

Together, the results from the Diversion Pool and Lowden Ranch support the view that gravel transport distances during an ordinary flow release are typically on the order of a few to several channel widths. This expectation can now be expanded to include flow releases with peaks as high as 8500 ft^3/s. However, much larger transport distances and gravel loads have been documented for flows that exceed that level by as little as 20%. This suggests that the 2015 flow release approached, but did not exceed, a threshold discharge above which bed mobility increases dramatically.

No adverse consequences of the 2015 gravel injections at either site were identified. Based on the 2015 data, both the Diversion Pool and the Lowden Ranch injection locations can therefore continue to be utilized as high-flow gravel injections locations. Due to the slow rate at which injected gravel appears to propagate downstream, however, we recommend that the TRRP attempt to identify additional augmentation sites and obtain the necessary environmental permitting in the near future. Use of additional augmentation locations would promote greater gravel dispersion, which would likely produce habitat benefits over longer stretches of the river.

Grain statistics extracted from photographs are considered to be accurate enough to be useful for long-term monitoring of bed surface conditions. Median and geometric mean particle sizes obtained by manual pebble counts on orthorectified substrate photographs tend to be slightly smaller than is obtained in field pebble counts, but are typically within about 10%.

Limited evidence suggests that the geometric mean may exhibit less negative bias than the median size. We recommend that TRRP periodically collect a library of substrate photographs at key locations to assess the long-term success of Program actions intended to increase the supply of mobile gravel downstream from Lewiston Dam.

Structure-from-motion photography is an effective method for compiling useful substrate photographs. This technology makes it possible to merge multiple ground-based photographs into a high-resolution orthorectified image of substrate over an area large enough to support statistically-valid sampling. Although photographs taken from ground level in the field must necessarily be slightly oblique, our experience with processing these data suggest that it is best to take photographs oriented as close to vertical as possible.

Performing pebble counts on photographs is labor-intensive, but appears to be necessary at present. A state-of-the-art computer script designed to automatically extract particle size information from photographs was found to produce inferior estimates of the median and mean particle sizes and to be wholly incapable of estimating the spread or shape of the particle size distribution. The use of automated algorithms is therefore not recommended at this time. Instead, we recommend visual inspection to perform rapid qualitative assessments of grain size changes supplemented by digital pebble counts for calibration/validation.

References

Ashmore, P.E. and M.A. Church. 1998. Sediment transport and river morphology: A paradigm for study, in *Gravel-bed Rivers in the Environment*, edited by P.C. Klingeman, R.L. Beschta, P.D. Komar and J.B. Bradley, Water Resources Publications, LLC. Highlands Ranch, CO, pp 115-148.

Bunte, K. and S.R. Abt. 2001a. Sampling frame for improving pebble count accuracy in coarse gravel-bed streams. *Journal of the American Water Resources Association* 37(4):1001-1014.

Bunte, K. and S.R. Abt. 2001b. *Sampling surface and subsurface particle-size distributions in wadable gravel- and cobble-bed streams for analyses in sediment transport, hydraulics, and streambed monitoring*. United States Forest Service, Rocky Mountain Research Station, General Technical Report RMRS-GTR-74.

Buscombe, D. 2013. Transferable wavelet method for grain-size distribution from images of sediment surfaces and thin sections, and other natural granular patterns. *Sedimentology* 60(7):1709-1732.

Church, M. 1995. Geomorphic response to river flow regulation: Case studies and time-scales. *Regulated Rivers: Research and Management* 11:3-22.

Church, M.A., D.G. McLean and J.F. Wolcott. 1987. River bed gravels: Sampling and analysis. In: *Sediment Transport in Gravel-bed Rivers*, C.R. Thorne, J.C. Bathurst and R.D. Hey, eds. Wiley.

Dietrich, W. E., J. W. Kirchner, H. Ikeda, and F. Iseya. 1989. Sediment supply and the development of the coarse surface layer in gravel-bedded rivers. *Nature* 340:215-217.

Folk, R.L. and W.C. Ward. 1957. Brazos River Bar: a study in the significance of grain size parameters. *Journal of Sedimentary Petrology* 27(1):3-26.

Gaeuman, D. 2011. *Water year 2010 implementation monitoring report*. Trinity River Restoration Program Technical Report TR-TRRP-2011-1, Weaverville, CA.

Gaeuman, D. and A. Krause, 2013. *Assessment of pool depth changes in the Trinity River between Lewiston Dam and the North Fork Trinity River*. Trinity River Restoration Program Technical Report TR-TRRP-2013-1, Weaverville, CA.

Gaeuman, D., 2014a. High-flow gravel injection for constructing designed in-channel features. *River Research and Applications*. doi:10.1002/rra.2662.

Gaeuman, D. 2014b. *Analyses to support gravel augmentation recommendations for the Trinity River, California*. Trinity River Restoration Program Technical Report TR-TRRP-2014-1, Weaverville, CA.

Gaeuman, D., B. Schmandt, and R.L. Stewart. 2016. *Seismic monitoring of bedload transport in a large gravel-bed river*, US Bureau of Reclamation, Denver, CO. Science and Technology Program Project No. 5561 Completion Report, ST-2016-5561-1.

Gaeuman, D. and R.L. Stewart. 2017. Sediment transport in the Trinity River, CA: Data systhesis 2004-2015. Trinity River Restoration Program Technical Report TR-TRRP-2017-1, Weaverville, CA.

GMA (Graham Matthews and Associates). 2012, *2010-2012 Trinity River bathymetric mapping*. Report to the Trinity River Restoration Program, Weaverville, CA.

GMA (Graham Matthews and Associates). 2015. *Trinity River 2013 gravel bar photo monitoring Report #3*, Report to the Trinity River Restoration Program, Weaverville, CA.

GMA (GMA Hydrology). 2016a. *2015 Diversion Pool survey report*, Report to the Trinity River Restoration Program, Weaverville, CA.

GMA (GMA Hydrology). 2016b. *2015 Trinity River sediment transport monitoring final report*. Report to the Trinity River Restoration Program, Weaverville, CA.

Gomez, B., R.L. Naff, and D.W Hubbell. 1989. Temporal Variations in Bedload Transport Rates Associated with the Mi-gration of Bedforms. *Earth Surface Processes and Land-forms* 14(2):135-156.

Grams, P.E., D.J. Topping, J.C. Schmidt, J.E. Hazel, Jr., and M. Kaplinski. 2013. Linking morphodynamic response with sediment mass balance on the Colorado River in Marble Canyon: Issues of scale, geomorphic setting, and sampling design. *Journal of Geophysical Research* 118(2):361-381, doi:10.1002/jgrf.20050.

Gray, J.R., J.D. Laronne, and J.D.G Marr. 2010. *Bedload-surrogate monitoring technologies*. U.S. Geological Survey Scientific Investigations Report 2010-5091, 37p.

Humphries, R., J.G. Venditti, and L.S. Sklar. 2012. Experimental evidence for the effect of hydrographs on sediment pulse dynamics in gravel-bedded rivers. *Water Resources Research* 48(1), doi:10.1029/2011WR010419.

Kondolf, G.M. and P.R. Wilcock, 1996. The flushing flow problem: Defining and evaluating objectives. *Water Resources Research* 32:2589-2599.

Lisle, T. E., J. E. Pizzuto, H. Ikeda, F. Iseya, and Y. Kodama. 1997. Evolution of a sediment wave in an experimental channel. *Water Resources Research* 33:1971-1981.

Marineau, M.D., J.T. Minear, and S.A. Wright. 2015. Using hydrophones as a surrogate monitoring technology to detect temporal and spatial variability in bedload transport. *Proceedings of the* 10th *Federal Interagency Sedimentation Conference*, April 19-23, 2015, Reno, NV.

Marineau, M.D., S.A. Wright, and D. Gaeuman. 2016. Comparison of sediment-generated noise measured using hydrophones to physical samples of bedload sediment in the Trinity River, California. *River Flows 2016: Proceedings of the 8th International Conference on Fluvial Hydraulics*, St. Louis, MO.

Milhous, R.T. 1998. Modelling of instream flow needs: The link between sediment and aquatic habitat. *Regulated Rivers: Research and Management* 14:79-94.

Parker, G. 1990. Surface-based bedload transport relation for gravel rivers. Journal of Hydraulic Research 28(4):417-436.

Petts, G.E. and I. Maddock. 1996. Flow allocation for in-river needs. In *River Restoration*, G.E. Petts and P. Calow, eds. Blackwell Science, London.

Richter, B.D., J.V. Baumgartner, R. Wigington and D.P. Braun. 1997. How much water does a river need? *Freshwater Biology* 37:231-249.

Ross, S.M. 2004. *Introduction to probability and statistics for scientists and engineers, 3rd edition*. Elsevier Academic Press, San Diego, California, 624 pp.

Schmandt, B., R.C. Aster, D. Scherler, V.C. Tsai, and K.E. Karlstrom. 2013. Multiple fluvial processes detected by seismic and infrasound monitoring of a controlled flood in the Grand Canyon. *Geophysical Research Letters* 40, doi:10.1002/grl.50953.

Schmandt, B., D. Gaeuman, R.L. Stewart, S.M. Hansen, V.C. Tsai, and J. Smith. (*Submitted*). Seismic array constraints on reach-scale bedload transport in the Trinity River. *Geology*.

Sklar, L.S., J. Fadde, J.G. Venditti, P. Nelson, M.A. Wydzga, Y. Cui, and W.E. Dietrich. 2009. Translation and dispersion of sediment pulses in flume experiments simulating gravel augmentation below dams. *Water Resources Research* 45, W08439, doi:10.1029/2008WR007346.

Stanford, J.A., J.V. Ward, W.J. Liss, C.A. Frissell, R.N. Williams, J.A. Lichatowich and C.C. Coutant. 1996. A general protocol for restoration of regulated rivers. *Regulated Rivers: Research and Management* 12:391-413.

TRRP and Essa Technologies, Ltd. 2009. *Integrated Assessment Plan Version 1.0*. Trinity River Restoration Program, Weaverville, CA.

USFWS and HVT (United States Fish and Wildlife Service and Hoopa Valley Tribe), 1999. *Trinity River Flow Evaluation Study*, Report to the Secretary of the Interior, US Department of the Interior, Washington, D.C.

Viparelli, E., D. Gaeuman, P.R. Wilcock, and G. Parker. 2011. A model to predict the evolution of a gravel bed river under an imposed cyclic hydrograph and its application to the Trinity River. *Water Resources. Research* 47, W02533, doi:10.1029/2010WR009164.

Watershed Sciences, Inc. 2012. *LiDAR remote sensing and orthophoto data collection: Trinity River, CA*. Final Report to the Trinity River Restoration Program.

Wohl, E. E., D. J. Anthony, S. W. Madsen, and D. M. Thompson 1996. A comparison of surface sampling methods for coarse fluvial sediments. *Water Resources. Research* 32(10):3219-3226.

Williams, G.P. and M.G Wolman. 1984. *Downstream Effects of Dams on Alluvial Rivers*. United States Geological Survey, Professional Paper 1286.

Wolman, M. G. 1954. A method of sampling coarse river-bed material. *American Geophysical Union Transactions* 35(6):951-956.